

# Exploiting Noise as a Resource for Computation and Learning in Spiking Neural Networks

Gehua Ma<sup>1</sup>, Rui Yan<sup>2</sup>, and Huajin Tang<sup>1,3,\*</sup>

<sup>1</sup>College of Computer Science and Technology, Zhejiang University, Hangzhou, P.R.C

<sup>2</sup>College of Computer Science and Technology, Zhejiang University of Technology, Hangzhou, P.R.C

<sup>3</sup>Lead contact

\*htang@zju.edu.cn

## Summary

Networks of spiking neurons underpin the extraordinary information-processing capabilities of the brain and have emerged as pillar models in neuromorphic intelligence. Despite extensive research on spiking neural networks (SNNs), most are established on deterministic models. Integrating noise into SNNs leads to biophysically more realistic neural dynamics and may benefit model performance. This work presents the noisy spiking neural network (NSNN) and the noise-driven learning rule (NDL) by introducing a spiking neuron model incorporating noisy neuronal dynamics. Our approach shows how noise may act as a resource for computation and learning and theoretically provides a framework for general SNNs. By incorporating various SNN architectures and algorithms, we show that our approach exhibits competitive performance and improved robustness against challenging perturbations than deterministic SNNs. Additionally, we demonstrate the utility of the NSNN model for neural coding studies. Overall, NSNN offers a powerful, flexible, and easy-to-use tool for machine learning practitioners and computational neuroscience researchers.

## Keywords

Spiking neural networks, noisy spiking neural networks, surrogate gradients, noise-driven learning, neuromorphic intelligence, neural coding

## Introduction

Spiking neural networks (SNNs) are seen as promising to bridge the gap between artificial and biological neural networks. They have been widely used as computational models in neuroscience research<sup>1,2</sup>. Benefiting from the recent progress in deep learning<sup>3-5</sup>, SNNs have also achieved remarkable advantages in various applications like computer vision and robotics<sup>6-15</sup>. In general, the majority of spiking neural models are established by deterministic SNNs (DSNNs), which ignore the inherent randomness of spiking neurons. Spiking neurons with noise-perturbed dynamics are considered more biologically realistic as the ion channel fluctuations and synaptic transmission randomness can cause noisy sub-threshold membrane voltages<sup>16-23</sup>. Furthermore, it incurs a potential benefit in generalization performance by promoting a more fault-tolerant representation space<sup>24-26</sup> and preventing overfitting<sup>27</sup>. However, a generic and flexible approach is required to fully exploit the noisy spiking neural models and comprehend the role of noise in networks of spiking neurons.

Previous literature<sup>28,29</sup> has investigated spiking neurons with stochastic activity by including a noise term in the differential equation of the membrane voltage. Such a noise term is typically modeled as white or colored noise derived in the stochastic differential equation with a diffusion process<sup>30,31</sup>. These approaches introduced detailed spiking models with noisy membrane dynamics; however, they do not attempt to build a generic method on the network level. Some studies<sup>32-35</sup> have presented small networks of noisy spiking neurons that can perform probabilistic inference. Nevertheless, these

methods are difficult to incorporate arbitrary network architectures due to the lack of an effective learning method. A recent study<sup>36</sup> introduced a Generalized Linear Model variant of the deterministic Spike Response Model, but their method also does not scale to deep SNNs of interest here. In deep SNNs, an ad-hoc solution called Surrogate Gradient Learning<sup>37–39</sup> (SGL, pseudo derivative<sup>40</sup>) has become the most widely used to solve the discontinuity when performing backpropagation<sup>41</sup>. While the surrogate gradient methods have proven highly effective<sup>42</sup>, they lack a theoretical foundation and a rational explanation<sup>43</sup>. In contrast, Neuroscientific-informed learning methods, like STDP<sup>44–46</sup>, are theoretically grounded and proven promising but struggle to work well in large networks and for complex tasks. It is therefore expected to develop an effective and scalable learning method like SGL while retaining insights regarding learning mechanisms like STDP.

The previous lack of a general computation and learning co-design of noisy spiking neural models limits their use. This prevents us from fully exploiting the performance of noisy spiking neural networks as machine learning models and exploring their potential as computational tools for neuroscience. Thus, this article aims to provide a generic and flexible integration of deep SNNs and noisy spiking neural models. In this way, we can make the spiking neural model biologically more realistic and get potential performance gains while being able to directly benefit from the engineering advances emerging in the rapidly-growing deep learning field. Moreover, in terms of theoretical value, this also demonstrates how noise may act as a resource for computation and learning in general networks of spiking neurons<sup>47</sup>.

Here, we show a noisy spiking neural network model (NSNN) using a noise-driven learning (NDL) paradigm. The approach exposed here provides a generic and flexible integration of noisy spiking neural models and deep SNNs. Additionally, NDL subsumes SGL and provides an insightful explanation for the latter. By incorporating various SNN architectures and algorithms, we demonstrate the effectiveness of NSNNs. Also, NSNNs lead to significantly improved robustness when facing challenging perturbations, such as adversarial attacks. In addition, through NSNN-based neural coding analyses, we show the potential of the NSNN model as a useful computational tool for neuroscientific research.

## Results

### Noisy spiking neural network and noise-driven learning

We consider a Noisy Leaky Integrate-and-Fire (LIF) spiking neuron model (**see Experimental Procedures** Method details) in this article, following previous literature that uses diffusion approximation<sup>30,31,48</sup>. It considers a discrete sub-threshold equation of the form:

$$\text{Noisy LIF sub-threshold dynamic: } u^t = \tau u^{t-1} + \phi_\theta(x^t) + \epsilon, \quad (1)$$

where  $u$  denotes membrane potential,  $x^t$  denotes input at time  $t$ ,  $\tau$  is the membrane time constant, and  $\phi_\theta$  is a parameterized input transform. The noise  $\epsilon$  is drawn from a zero-mean Gaussian distribution. Introducing internal noise induces a probabilistic firing mechanism (illustrated in Figure 1A), where the difference  $u - v_{\text{th}}$  governs the firing probability<sup>21,30,31</sup>:

$$\text{Noisy LIF probabilistic firing: } o^t \sim \text{Bernoulli}(\mathbb{P}[o^t = 1]), \quad (2)$$

where  $o^t$  is the spike state,  $\mathbb{P}[o^t = 1] = F_\epsilon(u^t - v_{\text{th}})$ ,  $F_\epsilon$  is the cumulative distribution function of the noise, and  $v_{\text{th}}$  is the firing threshold.

By employing Noisy LIF neurons, NSNN presents a general form of spiking neural networks. For instance, if the noise variance  $\text{Var}[\epsilon]$  approaches zero, the firing probability function  $F_\epsilon$  converges to the Heaviside step function, the Noisy LIF model, therefore, subsumes the deterministic LIF case.

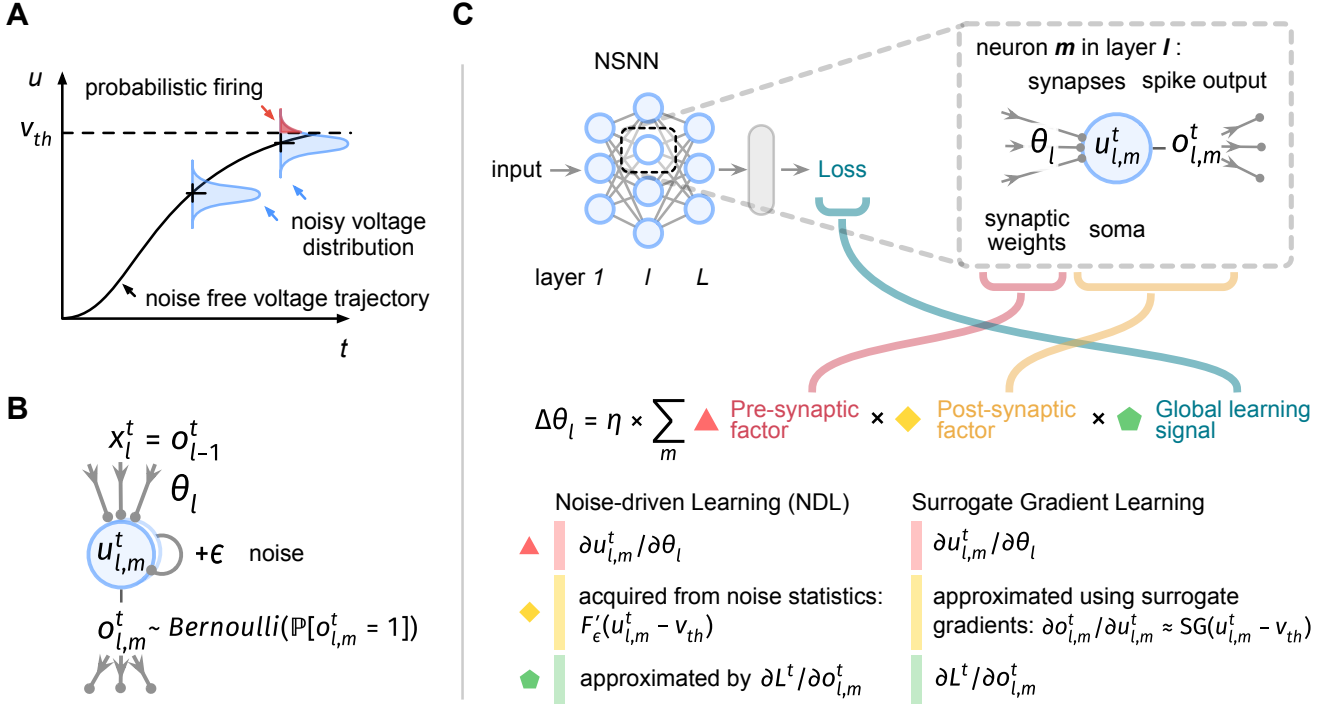


Figure 1: **Schemes for NSNN and NDL.** **A** Introducing noisy neuronal dynamics induces a probabilistic firing mechanism. The firing probability is given by the membrane noise cumulative distribution function, indicated by the shaded red part under the noisy voltage distribution.  $u$  denotes membrane voltage and  $v_{th}$  denotes firing threshold. **B** Computation flow in a Noisy LIF neuron  $l, m$  with membrane voltage  $u_{l,m}^t$ , input  $o_{l-1}^t$ , and output  $o_{l,m}^t$ . **C** Illustration of the computation for updating synaptic weights  $\theta_l$  of layer  $l$  using NDL and SGL.  $F'_\epsilon$  denotes the cumulative distribution function of noise  $\epsilon$ ,  $\eta$  denotes learning rate.

This suggests that conventional DSNs can be viewed as a special type of noisy spiking neural network. Further, by considering logistic membrane noise, the Noisy LIF neuron covers the sigmoidal neuron model<sup>47</sup>.

We then provide a well-defined solution of synaptic optimization via gradient descent for networks of spiking neurons. As noisy neurons code for binary variables, we may represent NSNNs using the Bayesian Network<sup>49,50</sup>, a probabilistic graphical model representing a set of variables and their conditional dependencies by a directed graph. Leveraging the Bayesian Network formulation, we can succinctly represent the spike states in NSNNs. This enables us to convert the gradient computation during synaptic optimization into gradient estimation in a probabilistic model, thereby circumventing the problematic firing function derivative. The resulting noise-driven learning (NDL) rule (**see Experimental Procedures** Method details) is illustrated in Figure 1C. In particular, the concise form of NDL makes it easy to combine with other online<sup>40,51</sup> or local learning<sup>52</sup> strategies to utilize computational resources more efficiently and handle more diverse tasks.

One noteworthy feature of NDL is providing a principled rationale for SGL. By leveraging the three-factor learning rule framework<sup>53,54</sup>, we show the mathematical relationship presented in Figure 1C, indicating that SGL can be regarded as a special type of NDL. Although the surrogate gradients<sup>7,37,38,42</sup> have been commonly associated with the straight-through estimator<sup>55–58</sup> in binarized networks, this association does not justify from the perspective of spiking neurons. In this sense, SGL appears to be an ad-hoc solution rather than a principled learning method<sup>37,43</sup>. NDL reveals the essence of the surrogate gradient, which is to obtain the post-synaptic learning factor from the neuron membrane noise statistics. Figure 2A illustrates the relationship between noise variance selection in NDL and surrogate gradient scale selection in SGL. When the noise variance is small, the probabilistic inference

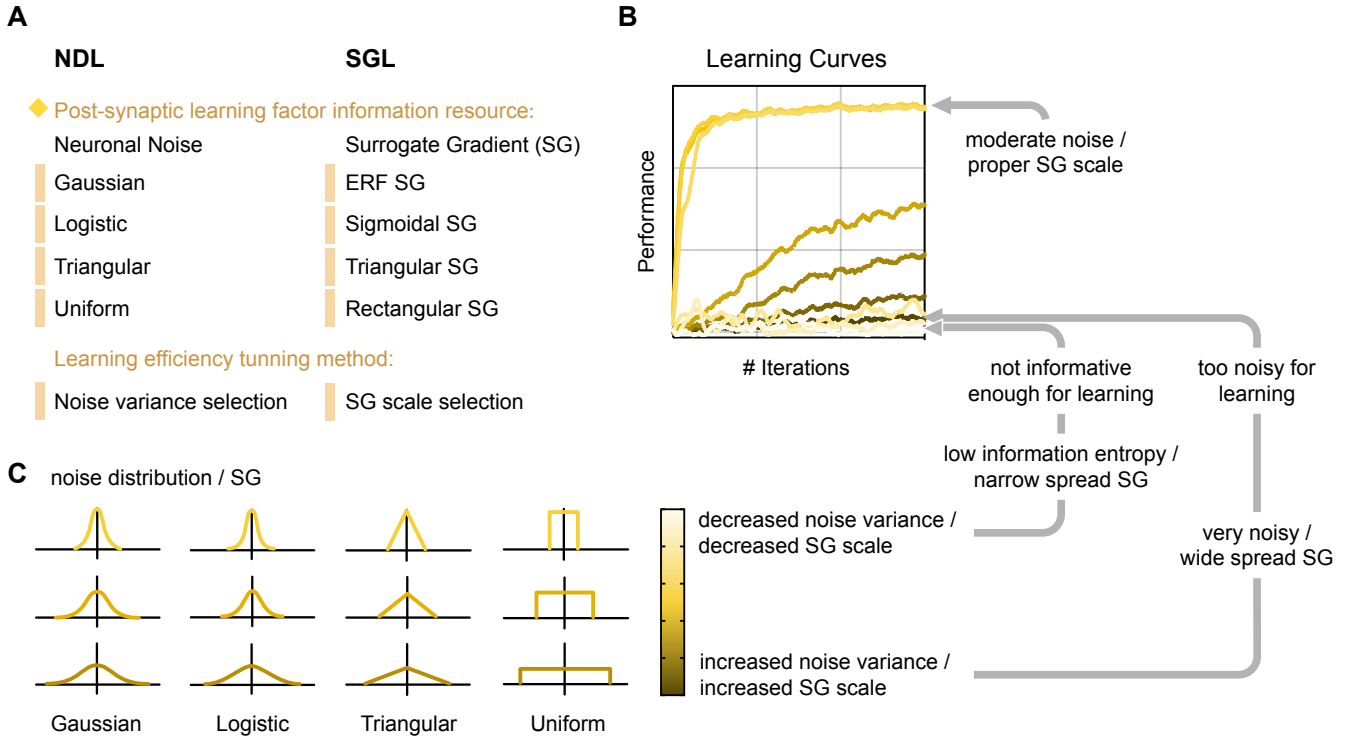


Figure 2: **NDL provides a principle backend for SGL.** **A** The correspondence between various types of neuronal noise and surrogate gradient functions. By using surrogate gradients, we are actually obtaining statistical information from the noisy membrane voltage dynamics to form a post-synaptic learning factor. **B, C** The effect of adjusting noise variance or surrogate gradient scale on learning efficiency.

forward of an NSNN can be approximated by the deterministic forward pass in a DSNN. Therefore, NDL derived within the NSNN framework subsumes SGL in conventional DSNNs. This also provides a random noise explanation for adjusting the scale (shape) of the surrogate gradient functions in SGL. Figures 2B and 2C visualize the impact of this variance selection or scale selection process on the learning effect of spiking neural networks, demonstrating that adjusting the scale of the surrogate gradient functions in SGL can be viewed as selecting noises with different variances in NDL.

## NSNN leads to high-performance spiking neural models

To verify the effectiveness and compatibility of NSNNs, we conducted experiments on multiple recognition benchmark datasets using various combinations of SNN architectures and algorithms. Recognition datasets we considered include static image datasets, including CIFAR-10 and CIFAR-100<sup>59</sup>, and event stream datasets collected using DVS cameras (silicon retina), including DVS-CIFAR<sup>60</sup> and DVS-Gesture<sup>61</sup>. More experimental details are presented in **Experimental Procedures** Experimental details.

We analyzed the accuracy of the models on these datasets, and we mainly focus on comparison with SNN models here. As shown in Table 1, results on CIFAR-10 and CIFAR-100 demonstrate the effectiveness of NSNNs on static image recognition tasks. For instance, on CIFAR-10, the NSNN model (with STBP, CIFARNet) achieved an accuracy of 0.9390 for two simulation timesteps, while its deterministic counterpart reported 0.9188. Our results indicate that NSNNs work well with various SNN architectures and algorithms, demonstrating great compatibility. Therefore, NSNNs can benefit from more efficient SNN algorithms or architectures. For example, when using the ResNet-18 architecture,

the NSNN model using the more efficient TET algorithm performs significantly better than the NSNN model using STBP (Table 1, CIFAR-10, CIFAR-100). NSNNs also demonstrate effectiveness and compatibility on event stream data recognition tasks (Table 1, DVS-CIFAR, DVS-Gesture) and outperformed their DSNN counterparts. In particular, on DVS-CIFAR data, the NSNN model with STBP and ResNet-19 significantly outperforms its DSNN counterpart, and performance improvements in other combinations are also evident. Due to the limited number of samples, DSNNs often experience severe overfitting when working with DVS-CIFAR and DVS-Gesture data. However, in NSNNs, internal noise improves the model's generalization ability, resulting in better performance than their deterministic counterparts. These generalization improvements brought about by internal noise in NSNNs align with previous research results in ANNs<sup>25–27</sup>.

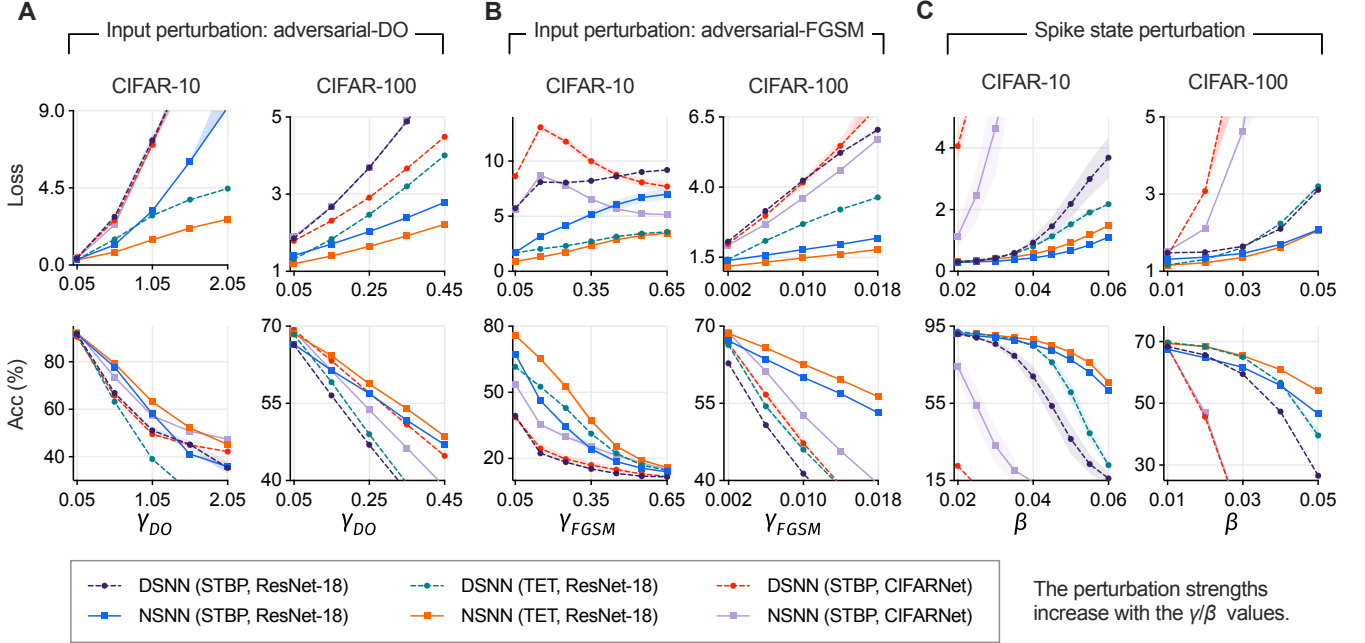


Figure 3: **Results of perturbed recognition experiments CIFAR-10 and CIFAR-100 datasets.** **A, B** Loss and accuracy results under input-level adversarial attacks (DO method, FGSM method). **C** Loss and accuracy results under spike state-level (firing state of spiking neurons) perturbations.

## NSNN leads to improved robustness against challenging perturbations

Robustness is essential for the information processing of spiking neural models to prevent external perturbations and interferences in real-world environments. From an application standpoint, robustness ensures reliable performance when facing corrupted input (possibly caused by errors in data collection and processing) and perturbed internal information flow (possibly caused by communication abnormalities between different units). In terms of building biologically realistic computational neural circuits, robust spiking neural models align more closely with the noisy yet resilient characteristics of biological circuits<sup>20,62,63</sup>.

Next, we demonstrate the improvement in robustness achieved by using NSNNs. To this end, we conducted perturbed recognition experiments on CIFAR-10, CIFAR-100, and DVS-CIFAR data (**see Experimental Procedures** Experimental details). We evaluated the performance of DSNNs and NSNNs by measuring their accuracy and loss values under various types and intensities of perturbations. The models were trained as described in the previous recognition experiments and tested using input-level or spike state-level perturbations.

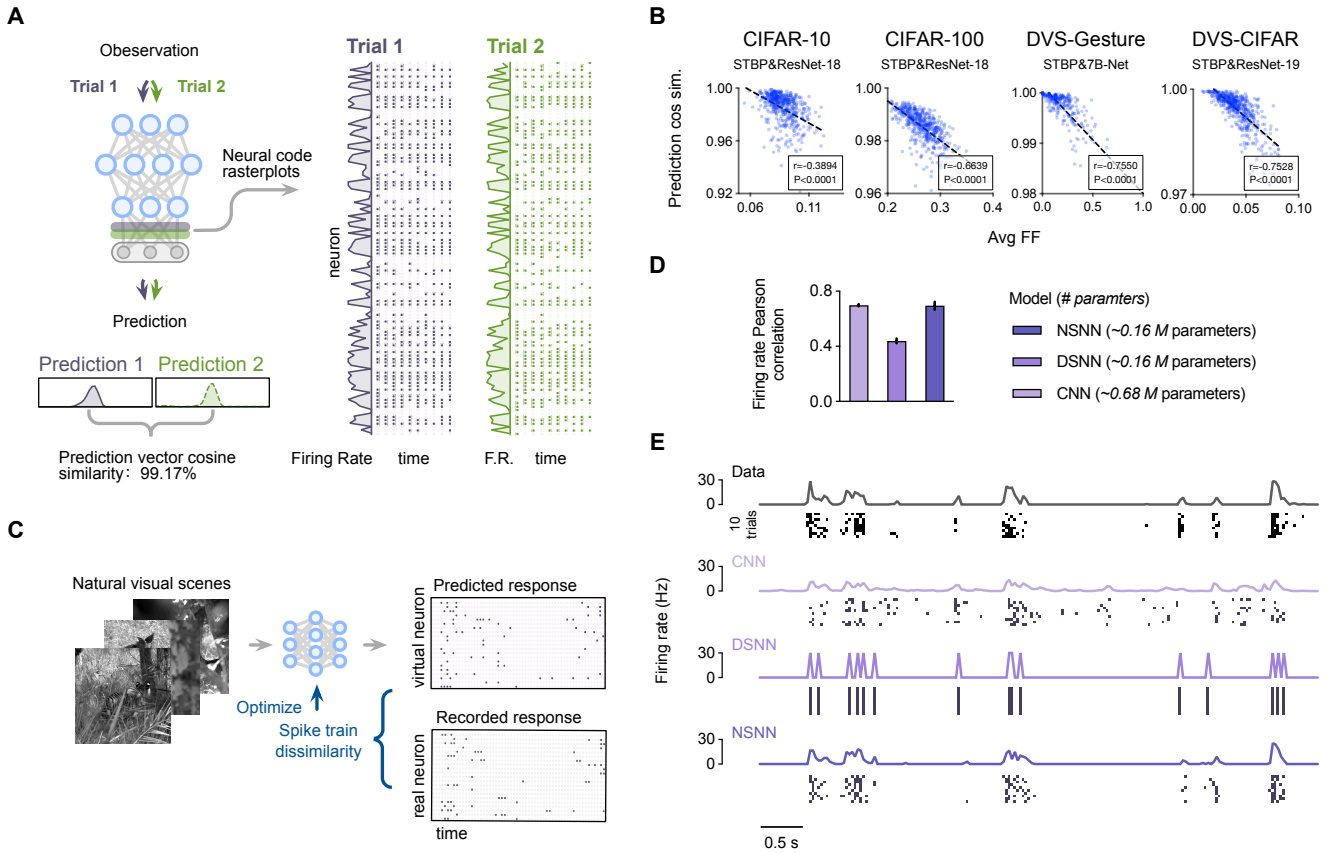
We considered several challenging input-level perturbations. For static image data CIFAR-10 and CIFAR-100, we used challenging adversarial attacks to construct corrupted inputs. This work leveraged two adversarial attacks: the Fast Gradient Sign Method (FGSM) and the Direct Optimization method (DO). For event stream data DVS-CIFAR, we used the EventDrop<sup>64</sup> perturbation, whose basic idea is randomly dropping a proportion of events with a probability of  $\rho$ . We also considered directly perturbing all spike states (firing states of spiking neurons) in SNNs to directly mimic the spike train variability in biological neural circuits. The intensity of the perturbation is controlled by a parameter  $\beta$ . Details are presented in **Experimental Procedures**.

Figure 3 shows that using NSNNs significantly improved robustness for static data recognition tasks (CIFAR-10, CIFAR-100). When facing challenging adversarial attacks and hidden-state perturbations, NSNN models consistently outperformed their DSNN counterparts. For example, in the CIFAR-100 FGSM adversarial attack experiment (Figure 3B), NSNNs demonstrated good resilience, whereas the reliability of DSNNs degraded radically as the perturbation intensity increased. Similarly, when facing direct interference with neuron spike states (Figure 3C), NSNNs exhibited superior robustness to their deterministic counterparts. The perturbed experiments on DVS-CIFAR data also showed that the NSNN model achieved better robustness than DSNNs (Tables 2, 3). When facing input-level EventDrop perturbations, NSNNs achieved lower loss and higher accuracy than their deterministic counterparts in most cases (Table 2). Similarly, as shown in Table 3, when facing hidden state perturbations, NSNNs demonstrated good resilience. Their superiority becomes apparent as the perturbation (spike state) level increases. For example, at a perturbation level of  $\beta = 0.01$  (with STBP and ResNet-19), the accuracy of NSNNs was 4.5% higher than that of DSNNs. When the perturbation level increased to 0.04, the accuracy lead of NSNNs over DSNNs reached 46.3%. We provide a theoretical analysis on internal noise and model stability in the following text (see **Experimental Procedures** Method details).

## NSNN demonstrates a promising tool for neural coding research

Although capturing the spike-based paradigm in neural circuits, conventional DSNNs failed to account for the reliability and variability in neural spike trains<sup>65,66</sup>, which limits their application as computational models in neural coding research. By contrast, NSNNs can faithfully recover prediction reliability and neural spike train variability, as shown in Figure 4A. The NSNN, therefore, demonstrates a useful tool for investigating neural coding, where to provide information about dynamic sensory cues, the patterns of action potentials in spiking neurons must be variable<sup>67</sup>.

We first show how NSNN can be used for neural coding analysis in spiking neural models. In particular, we leverage the NSNN model to provide empirical evidence for a rate coding strategy. Specifically, the internal randomness of NSNNs leads to slightly different neural codes (spike output of the final spiking layer) and predictions between trials given the same input (Figure 4A). This allows for analyzing the Pearson correlation between the variation in the firing rate of the neural code and the stability (reliability) of the final prediction in NSNNs. Since we consider a recognition task here, we use the output of the final spiking neuron layer, which contains more semantically informative data, as the neural code. We use the Fano Factor (FF) to numerically measure the firing rate variation in neural code and the cosine similarity of prediction vectors to measure prediction stability (see also **Experimental Procedures** Experimental details). A larger FF indicates greater firing rate variation between different trials, while high prediction cosine similarity corresponds to more stable predictive output. We find significant negative correlations between variation in firing rate and stability of prediction in learned NSNNs (Figure 4B). These results are robust to various combinations of SNN architectures and algorithms, suggesting that these NSNNs learn a primary rate coding-based policy. This makes sense as membrane noise injection introduces uncertainty into the firing process, reducing the reliability of precise spiking time-based coding. As the same firing rate (represented as firing count in



**Figure 4: NSNN-based coding analyses and experiments.** **A** NSNNs exhibit neural code-level variability and decision-level (prediction-level) reliability. We visualize the prediction distributions, spike rates, and raster plots of the final spiking layer outputs of two repeated trials obtained using DSV-CIFAR data. **B** Relationship between the average Fano Factor and prediction cosine similarity. Each dot represents a sample used for computing the Pearson correlation. The dotted line is a linear approximation. **C** Graphical illustration of the simple neural activity fitting experiment: spiking neural models were optimized to produce spike outputs close to the recorded neural activities. **D** The average firing rate Pearson correlation coefficients of different fitting models. Higher values indicate better predictions. **E** Spikes and firing rates of the recorded responses of a representative neuron and the predictions of three models (CNN, DSNN, NSNN) to a natural visual scene clip.

simulation steps here) can correspond to different spike trains, rate-based coding can improve model robustness by constructing a representation space with better fault tolerance.

Next, we perform a neural activity fitting task (see also **Experimental Procedures** Experimental details) using retinal neural recordings to natural visual scenes<sup>68</sup> (Figure 4C). We constructed DSNN and NSNN models with the same structure for this neural activity fitting task. These spiking neural models took the visual scenes as input and the recorded retinal responses as target outputs and were optimized to produce spike trains similar to recorded neural activity. To compare these spiking neural models with the current state-of-the-art, we also considered a competitive convolutional neural network (CNN) model<sup>69,70</sup> as the baseline. We evaluated the Pearson correlation coefficient between the recorded and predicted neural activity to compare the performances of these models numerically. To illustrate that the DSNN model failed to account for variability in the neural activity of interest, we show in Figure 4E the spike rasters and firing rates of a representative neuron. As presented in Figure 4E, the DSNN model could not reproduce the variable spike patterns and failed to fit real firing rate curves accurately. In contrast, we observed a significant improvement by using NSNNs (Figure 4D).



The NSNN model performs well in fitting both spike activity and firing rate. Additionally, the NSNN model can demonstrate competitive performance with fewer model parameters than the CNN model. These results demonstrate that by applying performance optimization to a biologically appropriate NSNN model, it is possible to construct quantitative predictive models of neural coding<sup>71</sup>.

## Discussion

In this study, we reported noisy spiking neural models and noise-driven learning by exploiting neuronal noise as a resource for computation and learning in networks of spiking neurons. We introduced a membrane noise term into the deterministic spiking neuron model<sup>28,31,72</sup>, formulated the networks of these noisy spiking neurons, and derived the NDL learning method to perform synaptic optimization. Our results on multiple datasets indicate that NSNNs exhibit competitive performance and improved generalization ability. Further perturbed tests show that NSNNs demonstrate improved robustness against various perturbations, including challenging adversarial attacks, thereby providing support for the internal noise-model stability analysis. Besides, NSNNs can easily integrate with various SNN algorithms and network architectures, allowing our methodology to be trivially generalized to a wide range of fields that require the presence of stochasticity. Finally, we deliberated from the coding strategy analysis and building predictive coding models as an illustration and demonstrated that NSNNs provide a promising tool for neural coding research.

This work presents a novel approach for constructing and training spiking neural networks. The NSNN framework enables the flexible integration of internal noise with different distributions and variances into SNN models. In machine learning, introducing internal noise typically offers performance benefits, such as preventing overfitting and enhancing model robustness. As such, NSNNs can be utilized to obtain better performance models. The computation and learning form of NSNN incorporated with NDL is concise and straightforward, making it easy to implement in larger network architectures using simple module replacement based on the DSNN implementation. Here we demonstrate that the combination of NSNN and NDL can be well incorporated with representative network architectures and algorithms. Going forward, NSNNs can easily be integrated with larger models, like spiking transformers<sup>73,74</sup>. Although we currently assign credits along the temporal dimension using back-propagation through time in experiments, NDL is compatible with potential online or local learning methods. Further research into the noisy spiking neural models may provide insights for designing local, online learning mechanisms<sup>40,51,52</sup> and combining them with NDL to form more biophysically-plausible SNN learning methods. As such, NSNN presents a promising avenue for advancing spiking neural networks and their learning methods.

Spiking neural models are popular in neuroscience research for their biologically realistic spike-based computation paradigm. However, conventional deterministic spiking neural models cannot account for the variability in neural spike trains<sup>67</sup>. Therefore, research into the noisy spiking neural model, which aims to provide a useful tool at a computational level, has practical benefits for computational neuroscience. For instance, NSNNs can be used for neuron type<sup>2,75</sup>, neural system identification<sup>76,77</sup>, and constructing predictive counterparts of neural circuits<sup>78,79</sup>. In experiments exposed in this article, we mainly focus on the potential application of NSNNs in neural coding. This a popular research topic in neuroscience and other fields such as computer vision, neuromorphic computing, neural prosthesis, and brain-computer interface. Our results indicate that NSNNs are able to recover reliability and variability in neural circuits. Notably, NSNNs achieved competitive performance with fewer parameters than conventional ANN models in the task of fitting neural responses to natural visual scenes. As such, NSNN provides a promising tool for building computational accounts for various sensory neural circuits and will enable richer models of complex neural computations in the brain.

In summary, the NSNN model introduced in this study demonstrates great potential for advancing



spiking neural network research and inspiring the development of artificial intelligence algorithms and neuromorphic models. The approach taken in this paper paves the way toward better computational tools by enabling richer models of complex spiking computations for computational neuroscience research. These models will facilitate a deeper understanding of neural computations and uncover neural processing mechanisms.

## EXPERIMENTAL PROCEDURES

### Resource availability

#### Lead contact

Further information and requests for resources should be directed to and will be fulfilled by the lead contact, Prof. Huajin Tang (htang@zju.edu.cn).

#### Materials availability

This study did not generate new unique reagents.

#### Data and code availability

All data used in this paper are publicly available and can be accessed at <https://www.cs.toronto.edu/~kriz/cifar.html> for the CIFAR (CIFAR-10, CIFAR-100) dataset, <https://research.ibm.com/interactive/dvsgesture/> for the DVS128 Gesture (DVS-Gesture) dataset, and [https://figshare.com/articles/dataset/CIFAR10-DVS\\_New/](https://figshare.com/articles/dataset/CIFAR10-DVS_New/) for the CIFAR10-DVS (DVS-CIFAR) dataset. The code can be found at <https://github.com/genema/Noisy-Spiking-Neuron-Nets> (<https://doi.org/10.5281/zenodo.7986394>).

### Method details

#### Notations

We use  $x, u, o$  to represent input, membrane potential, and spike output. Also,  $x_{l,m}^t, u_{l,m}^t, o_{l,m}^t$  denote variables of neuron  $m$  in layer  $l$  (whose dimension is  $\dim(l) = \dim(x_l)$ ) at time  $t$ , where  $l \in [1, L]$  and  $t \in [1, T]$ . We also use boldface type to represent the sets or matrices of variables, e.g., variables of layer  $l$  at timestep  $t$  are marked as  $\mathbf{x}_l^t, \mathbf{u}_l^t, \mathbf{o}_l^t$ . Spike state space is marked as  $\mathbb{S}$ . Notations  $\mathbb{E}[\cdot], \mathbb{P}[\cdot], p(\cdot)$  and  $F(\cdot)$  are, respectively, expectation, probability, probability distribution, and cumulative distribution function.

#### LIF neuron

We consider the commonly used Leaky Integrate-and-Fire (LIF) neuron model<sup>80,81</sup> in this work, which describes the sub-threshold membrane potential dynamics as

$$\tau_m \frac{du}{dt} = -(u - u_{\text{reset}}) + RI(t), u < v_{\text{th}}, \quad (3)$$

where  $R, \tau_m$  are membrane resistance and time constant,  $I$  is the input current and  $v_{\text{th}}, u_{\text{reset}}$  are firing threshold, resting potential, respectively. It leads to the following discrete-time computational form in

practice<sup>7,82</sup>:

$$\begin{aligned} \text{sub-threshold dynamic: } u^t &= \tau u^{t-1} + \phi_\theta(x^t), \\ \text{firing: } o^t &= \text{spike}(u^t, v_{\text{th}}) \triangleq \text{Heaviside}(u^t - v_{\text{th}}), \\ \text{resetting: } u^t &= u^t \cdot (1 - o^t) + u_{\text{reset}}, \end{aligned} \quad (4)$$

where  $x^t$  is the input at time  $t$ ,  $\tau$  is the membrane time constant,  $\phi_\theta : \mathbb{S}^{\dim(x^t)} \rightarrow \mathbb{R}$  denotes a parameterized input transform. To introduce a simple model of neuronal spiking and refractoriness, we assume  $v_{\text{th}} = 1$ ,  $\tau = 0.5$  and  $u_{\text{reset}} = 0$  throughout this research.

## Noisy LIF neuron

The Noisy LIF presented here is based on previous works that use diffusive approximation<sup>30,31,48</sup>, where the sub-threshold dynamic is described by the Ornstein-Uhlenbeck process<sup>83,84</sup>:

$$\begin{aligned} \tau_m \frac{du}{dt} &= -(u - u_{\text{reset}}) + RI(t) + \xi(t), \text{ e.q.} \\ du &= -(u - u_{\text{reset}}) \frac{dt}{\tau_m} + RI(t) \frac{dt}{\tau_m} + \sigma dW^t, \end{aligned} \quad (5)$$

the white noise  $\xi$  is a stochastic process,  $\sigma$  is the amplitude of the noise and  $dW^t$  are the increments of the Wiener process in  $dt$ <sup>31</sup>. As  $\sigma dW^t$  are random variables drawn from a zero-mean Gaussian, this formulation is directly applicable to discrete-time simulations. Specifically, using the Euler-Maruyama method, we get a Gaussian noise term added on the right-hand side of Equation 4. Without loss of generality, we extend the additive noise term in the discrete form to general continuous noise<sup>85</sup>, by Equation 4, the sub-threshold dynamic of Noisy LIF can be described as:

$$\text{Noisy LIF sub-threshold dynamic: } u^t = \tau u^{t-1} + \phi_\theta(x^t) + \epsilon, \quad (6)$$

where the noise  $\epsilon$  is independently drawn from a known distribution that satisfies  $\mathbb{E}[\epsilon] = 0$  and  $p(\epsilon) = p(-\epsilon)$ . Equation 6 can also be obtained by discretizing an Itô stochastic differential equation variant of LIF neurons<sup>23,86</sup>. We consider in this article Gaussian noise for all Noisy LIF neurons.

The membrane potentials and spike outputs become random variables due to the injection of random noises. Using noise as a medium, we naturally obtain the firing probability distribution of Noisy LIF based on the threshold firing mechanism:

$$\begin{aligned} \mathbb{P}[\text{firing}] &= \mathbb{P}[\underbrace{u^t + \epsilon}_{\text{Threshold firing}} > v_{\text{th}}] \\ &= \mathbb{P}[\underbrace{\epsilon < u^t - v_{\text{th}}}_{\text{cumulative distribution function definition}}] \triangleq F_\epsilon(u^t - v_{\text{th}}). \end{aligned} \quad (7)$$

Therefore,

$$o^t = \begin{cases} 1, & \text{with probability } F_\epsilon(u^t - v_{\text{th}}), \\ 0, & \text{with probability } 1 - F_\epsilon(u^t - v_{\text{th}}). \end{cases} \quad (8)$$

The expressions above show how noise acts as a resource for computation<sup>47</sup>. Thereby, we can formulate the firing process of Noisy LIF as

$$\text{Noisy LIF probabilistic firing: } o^t \sim \text{Bernoulli}(F_\epsilon(u^t - v_{\text{th}})). \quad (9)$$

Specifically, it relates to previous literature on escape noise models<sup>30,87,88</sup>, in which the difference  $u - v_{\text{th}}$  governs the neuron firing probabilities<sup>21,31</sup>. In addition, Noisy LIF employs the same resetting mechanism as the LIF model. Unless otherwise indicated, we focus on the discrete form in this research, which is of practical interest.

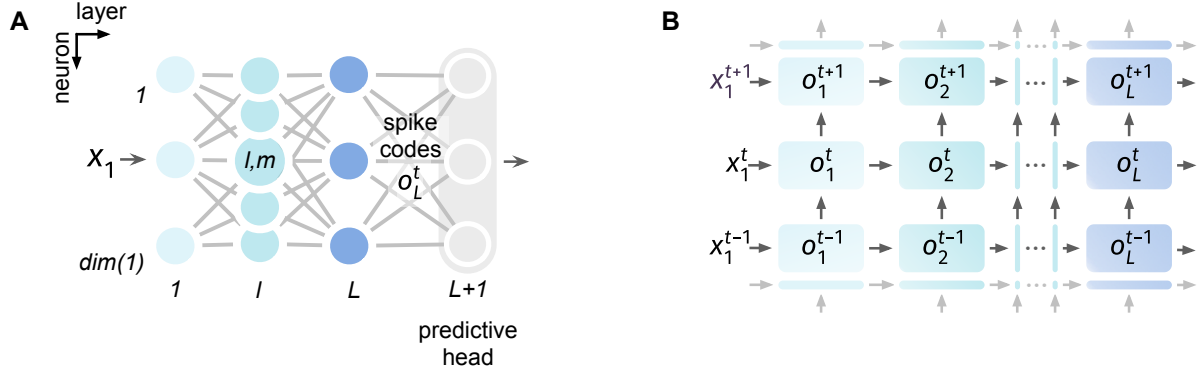


Figure 5: **Graphical illustrations of NSNN.** **A** NSNN graphical illustration with neuron, layer notations. **B** Assumed dependencies between spike states using the Bayesian Network frame.

### Noisy Spiking Neural Network

We consider the NSNN model as a probabilistic recognition model here as an example. Let  $x_1^t$  denote the input at time  $t$ , using the dynamics of Noisy LIF in Equations 6-9, an NSNN consists of  $L+1$  layers is given by

$$\begin{aligned} \text{input layer: } x_1^t &= x_1^t, u_1^t = \tau u_1^t + \Phi_{\theta_1}(x_1^t) + \epsilon_1, o_1^t = \{o_{1,m}^t : o_{1,m}^t \sim \text{Bernoulli}(\mathbb{P}[o_{1,m}^t = 1])\}_{m=1}^{\dim(1)}, \\ \text{hidden layer: } x_l^t &= o_{l-1}^t, u_l^t = \tau u_l^t + \Phi_{\theta_l}(x_l^t) + \epsilon_l, o_l^t = \{o_{l,m}^t : o_{l,m}^t \sim \text{Bernoulli}(\mathbb{P}[o_{l,m}^t = 1])\}_{m=1}^{\dim(l)}, \\ \text{predictive head: } \mathcal{L} &= f_{\theta_{L+1}}(o_L^t) = f(\Phi_{\theta_{L+1}}(o_L^t)). \end{aligned} \quad (10)$$

The output  $o_l^t$  of layer  $l$  is a representation vector in the spike space  $\mathbb{S}^{\dim(l)}$ , the membrane potentials  $u_l^t \in \mathbb{R}^{\dim(l)}$ , and the mapping  $\Phi_{\theta_l} : \mathbb{S}^{\dim(l-1)} \rightarrow \mathbb{R}^{\dim(l)}$ . The noise vector  $\epsilon_l \in \mathbb{R}^{\dim(l)}$  consists of independent random noise with a known distribution (Gaussian in this article). The predictive head  $f_{\theta_{L+1}}(o_L^t)$  includes a parameterized mapping  $\phi_{\theta_{L+1}}(o_L^t)$  and a loss function  $f$ , denoting the part that decodes predictions from the neural representation  $o_L^t$  and compute the loss value.  $\phi_{\theta_l}$  represents a map like fully connected or convolution and is thus differentiable w.r.t. parameter  $\theta_l$ . Dividing the synaptic parameters by layers, as mentioned above, results in no loss of generality as they can be defined as any differentiable mapping.

For example, to solve recognition problems, we shall consider the predictive probability model  $p_{\theta_{L+1}}(y|o_L^t) = \text{softmax}(\phi_{\theta_{L+1}}(o_L^t))$ , where the map  $\phi_{\theta_{L+1}}$  computes the predictive scores using the neural representation  $o_L^t$ . The function  $f$  can be the cross-entropy of the predictive distribution  $p_{\theta_{L+1}}(y|o_L^t)$  and the target distribution  $p_{\text{target}}(y|x_1^t)$ . Note that  $f_{\theta_{L+1}}(o_L^t)$  here computes the instantaneous loss, different from the  $\frac{1}{T} \sum_t f^t$ , which is computed over the entire time window and ignores potential online learning<sup>82</sup>.

Since each neuron codes for a random variable  $o_{l,m}^t$ , we can describe the NSNN by the Bayesian Network model and represent the joint distribution of all spike states given input  $x_1^t$  as

$$p_{\theta}(o_{1...L}^t | x_1^t, o_{1...L}^{t-1}) = p_{\theta_1}(o_1^t | x_1^t, o_1^{t-1}) \prod_{l=2}^L p_{\theta_l}(o_l^t | o_{l-1}^t, o_l^{t-1}), \quad (11)$$

where the layer representation is  $p_{\theta_l}(o_l^t | o_{l-1}^t, o_l^{t-1}) = \prod_{m=1}^{\dim(l)} p_{\theta_{l,m}}(o_{l,m}^t | o_{l-1}^t, o_{l,m}^{t-1})$ .

## Noise-driven Learning

To perform NSNN synaptic optimization, the central problem is to estimate the gradient of the expected loss  $\mathbb{E}_{\mathbf{o}_{1:L}^t}[\mathcal{L}]$ . By Equations 10, 11,  $g_l$  is given by:

$$g_l = \nabla_{\theta_l} \mathbb{E}_{\mathbf{o}_{1:L}^t}[\mathcal{L}] = \nabla_{\theta_l} \sum_{\mathbf{o}_{1:L}^t} p_{\theta}(\mathbf{o}_{1:L}^t | \mathbf{x}_1^t, \mathbf{o}_{1:L}^{t-1}) f_{\theta_{L+1}}(\mathbf{o}_L^t). \quad (12)$$

As Equation 12 is intractable to compute, we expect an estimation so that the parameters can be tuned using gradient-based routines.

The dimensionality of the spike state space is rather limited (either spike or silence). Leveraging this property, we can derive an estimator by conditioning (local marginalization), which performs exact summation over a single random variable to reduce variance<sup>89,90</sup>. We first factorize the joint distribution  $p_{\theta}(\mathbf{o}_{1:L}^t | \mathbf{x}_1^t, \mathbf{o}_{1:L}^{t-1})$  as the product of  $\prod_{i \neq l} p_{\theta_i}(\mathbf{o}_i^t | \mathbf{o}_{i-1}^t, \mathbf{o}_i^{t-1})$ ,  $\prod_{k \neq m} p_{\theta_l}(\mathbf{o}_{l,k}^t | \mathbf{o}_{l-1}^t, \mathbf{o}_{l,k}^{t-1})$  and  $p_{\theta_l}(\mathbf{o}_{l,m}^t | \mathbf{o}_{l-1}^t, \mathbf{o}_{l,m}^{t-1})$ . Then, Equation 12 becomes

$$g_l = \sum_{\mathbf{o}_{1:L}^t} \sum_m \left( \prod_{i \neq l} p_{\theta_i}(\mathbf{o}_i^t | \mathbf{o}_{i-1}^t, \mathbf{o}_i^{t-1}) \prod_{k \neq m} p_{\theta_l}(\mathbf{o}_{l,k}^t | \mathbf{o}_{l-1}^t, \mathbf{o}_{l,k}^{t-1}) \right) \nabla_{\theta_l} p_{\theta_l}(\mathbf{o}_{l,m}^t | \mathbf{o}_{l-1}^t, \mathbf{o}_{l,m}^{t-1}) f_{\theta_{L+1}}(\mathbf{o}_L^t). \quad (13)$$

Using the fact  $\mathbb{P}[\mathbf{o}_{l,m}^t = 0] = 1 - \mathbb{P}[\mathbf{o}_{l,m}^t = 1]$ , we have that

$$\sum_{\mathbf{o}_{l,m}^t} \nabla_{\theta_l} p_{\theta_l}(\mathbf{o}_{l,m}^t | \mathbf{o}_{l-1}^t, \mathbf{o}_{l,m}^{t-1}) f_{\theta_{L+1}}(\mathbf{o}_L^t) = \nabla_{\theta_l} p_{\theta_l}(\mathbf{o}_{l,m}^t | \mathbf{o}_{l-1}^t, \mathbf{o}_{l,m}^{t-1}) \Delta \mathcal{L}, \quad (14)$$

where the loss difference term  $\Delta \mathcal{L} = f_{\theta_{L+1}}(\mathbf{o}_L^t) - f_{\theta_{L+1}}(\mathbf{o}_{l,m}^{t-1})$ , here we use  $\mathbf{o}_{l,m}^{t-1}$  to denote the new state  $\mathbf{o}_L^t$  if  $\mathbf{o}_{l,m}^t$  changes. Given that  $\sum_{\mathbf{o}_{l,m}^t} p_{\theta_l}(\mathbf{o}_{l,m}^t) = 1$  and using Equations 13, 14, we have

$$g_l = \sum_{\mathbf{o}_{1:L}^t} \left( \prod_{i=1}^L p_{\theta_i}(\mathbf{o}_i^t | \mathbf{o}_{i-1}^t, \mathbf{o}_i^{t-1}) \right) \hat{g}_l = \mathbb{E}_{\mathbf{o}_{1:L}^t} [\hat{g}_l], \quad (15)$$

where

$$\hat{g}_l = \sum_m \nabla_{\theta_l} p_{\theta_l}(\mathbf{o}_{l,m}^t | \mathbf{o}_{l-1}^t, \mathbf{o}_{l,m}^{t-1}) \Delta \mathcal{L}. \quad (16)$$

Intuitively, this local gradient is defined as a sum of the contributions of all neurons in layer  $l$ . To get an estimate of  $g_l$ , we can simply sample from  $p_{\theta}(\mathbf{o}_{1:L}^t | \mathbf{x}^t)$  and calculate using Equation 16. However, it is still unwise to compute  $\Delta \mathcal{L}$  as it requires repeated evaluations and, thus, cannot scale to large models<sup>91</sup>. Inspired by previous studies<sup>91-93</sup>, we may attribute the change of loss value to the state flip of variable  $\mathbf{o}_{l,m}^t$ . By doing so, we may approximate the loss difference  $\Delta \mathcal{L}$  when the state of  $\mathbf{o}_{l,m}^t$  alters using a first-order approximation:

$$\Delta \mathcal{L} \approx (\mathbf{o}_{l,m}^t - (1 - \mathbf{o}_{l,m}^{t-1})) \frac{\partial f_{\theta_{L+1}}}{\partial \mathbf{o}_{l,m}^t} = (2\mathbf{o}_{l,m}^t - 1) \nabla_{\mathbf{o}_{l,m}^t} f_{\theta_{L+1}}. \quad (17)$$

Note that this approximation introduces bias to the gradient estimator, except when the map  $f$  is multilinear<sup>91,93</sup>. By Equations 16, 17, we have that

$$\hat{g}_l = \sum_m \nabla_{\theta_l} p_{\theta_l}(\mathbf{o}_{l,m}^t | \mathbf{o}_{l-1}^t, \mathbf{o}_{l,m}^{t-1}) (2\mathbf{o}_{l,m}^t - 1) \nabla_{\mathbf{o}_{l,m}^t} f_{\theta_{L+1}}. \quad (18)$$

By Equation 8, we have that  $\nabla_{\theta_l} p_{\theta_l}(\mathbf{o}_{l,m}^t | \mathbf{o}_{l-1}^t, \mathbf{o}_{l,m}^{t-1}) = (2\mathbf{o}_{l,m}^t - 1) F'_{\epsilon}(u_{l,m}^t - v_{th}) \nabla_{\theta_l} u_{l,m}^t$ . Therefore, by Equation 18, we can formulate the noise-driven learning rule as<sup>53,54</sup>

$$\text{NDL: } \hat{g}_l = \sum_m \underbrace{\nabla_{\theta_l} u_{l,m}^t}_{\text{Pre-synaptic factor}} \underbrace{F'_{\epsilon}(u_{l,m}^t - v_{th})}_{\text{Post-synaptic factor}} \underbrace{\nabla_{\mathbf{o}_{l,m}^t} f_{\theta_{L+1}}}_{\text{Global learning signal}}. \quad (19)$$

Computing synaptic weights update using Equation 19 does not require calculating an additional gradient generator in the forward pass, and  $\hat{g}_l$  can be computed layer by layer in a single backward passage. Specifically, the gradient estimation is performed by a backward pass, where the  $\nabla_{u_{l,m}^t} o_{l,m}^t$  term in the exact chain rule is replaced by a term computed using the noise probability density function  $F'_\epsilon$ . Therefore, NDL is easy to implement and can mesh well with modern automatic differentiation frameworks. And, since NDL is backpropagation-compatible, we can use it to optimize NSNNs of any architecture easily.

Interestingly, some previous works<sup>94</sup> also constructed a surrogate gradient function (pseudo derivative to surrogate the  $\nabla_{u_{l,m}^t} o_{l,m}^t$ ) by empirically adding infinitesimal Gaussian perturbations to the spiking neuron. The surrogate gradient function obtained by their single-neuron analysis shares similar insights as the post-synaptic term in NDL. However, our results are obtained from a network-level derivation.

### Theoretical analyses on internal noise and stability

Next, we analyze the stability of continuous NSNN sub-threshold dynamics. Our analytical results show that the internal noise in NSNNs can benefit the stability against small perturbations by allowing faster self-correction. This will also offer another lens through which to highlight the potential of NSNNs for improved performance and robustness<sup>62</sup>. To preface the analyses, we model an NSNN layer as a special case of a stochastic system consisting of one drift term  $f$  (to model the deterministic part) and one diffusion term  $g$  (to model the stochastic part), formally,

$$d\mathbf{u}^t = f(\mathbf{u}^t, \mathbf{I}^t)dt + g(\mathbf{u}^t, \mathbf{I}^t)d\mathbf{W}^t, \quad (20)$$

where  $\mathbf{u}^t, \mathbf{I}^t \in \mathbb{R}^{\dim(\mathbf{u}^t)}$ ,  $\mathbf{W}^t$  is a  $\dim(\mathbf{u}^t)$ -dimensional Wiener process. And the coefficient  $f, g$  satisfy the following assumption.

**Assumption** *There exists a constant  $K > 0$  such that  $\|f(\mathbf{u}_1^t, t) - f(\mathbf{u}_2^t, t)\| + \|g(\mathbf{u}_1^t, t) - g(\mathbf{u}_2^t, t)\| \leq K\|\mathbf{u}_1^t - \mathbf{u}_2^t\|$  for all  $\mathbf{u}_1^t, \mathbf{u}_2^t \in \mathbb{R}^{\dim(\mathbf{u}^t)}$ ,  $t \in \mathbb{R}^+$ .*

In particular, we focus on the choice of  $f$  and  $g$ :

$$\begin{aligned} f(\mathbf{u}^t, \mathbf{I}^t) &= a_1 \mathbf{u}^t + \mathbf{B}_1 \mathbf{I}^t, \\ g(\mathbf{u}^t, \mathbf{I}^t) &= a_2 \text{diag}(1) + b_2 f(\mathbf{u}^t, \mathbf{I}^t), \end{aligned} \quad (21)$$

with constants  $a_1 \in \mathbb{R}$ ,  $a_2, b_2 \in [0, \infty)$  and matrix  $\mathbf{B}_1 \in \mathbb{R}^{\dim(\mathbf{u}^t) \times \dim(\mathbf{I}^t)}$ . We can recover an NSNN layer consisting of Noisy LIF neurons described in the main text by letting  $a_1 = -1/\tau_m$ ,  $a_2 = \sigma$  and  $b_2 = 0$ .

Further, consider initializing the system represented by Equations 20,21 with two slightly different initializations  $\mathbf{u}^0, \mathbf{u}_e^0 \triangleq \mathbf{u}^0 + \boldsymbol{\varepsilon}^0$ , where  $\boldsymbol{\varepsilon}^0 \in \mathbb{R}^{\dim(\mathbf{u})}$  is the initial external perturbation (error) on membrane potentials. Then, the evolution of error  $\boldsymbol{\varepsilon}^t = \mathbf{u}_e^t - \mathbf{u}^t$  satisfies the SDE

$$d\boldsymbol{\varepsilon}^t = \Delta f(\boldsymbol{\varepsilon}^t)dt + \Delta g(\boldsymbol{\varepsilon}^t)dt, \quad (22)$$

where

$$\begin{aligned} \Delta f(\boldsymbol{\varepsilon}^t) &\triangleq (f(\mathbf{u}^t + \boldsymbol{\varepsilon}^t, \mathbf{I}^t) - f(\mathbf{u}^t, \mathbf{I}^t)), \\ \Delta g(\boldsymbol{\varepsilon}^t) &\triangleq (g(\mathbf{u}^t + \boldsymbol{\varepsilon}^t, \mathbf{I}^t) - g(\mathbf{u}^t, \mathbf{I}^t)). \end{aligned} \quad (23)$$

Here we assume that the two random processes  $\mathbf{u}^t, \mathbf{u}_e^t = \mathbf{u}^t + \boldsymbol{\varepsilon}^t$  are driven by the same Wiener process to make the subtraction operation valid. Since  $\Delta f(0) = 0$  and  $\Delta g(0) = 0$ ,  $\boldsymbol{\varepsilon}^t = 0$  admits a trivial solution for Equation 22, whose uniqueness is guaranteed by Assumption 1<sup>95</sup>. We focus on analyzing the stability of the trivial solution  $\boldsymbol{\varepsilon}^t = 0$ ; if it is stable, small initial perturbation  $\boldsymbol{\varepsilon}^0 \neq 0$  will

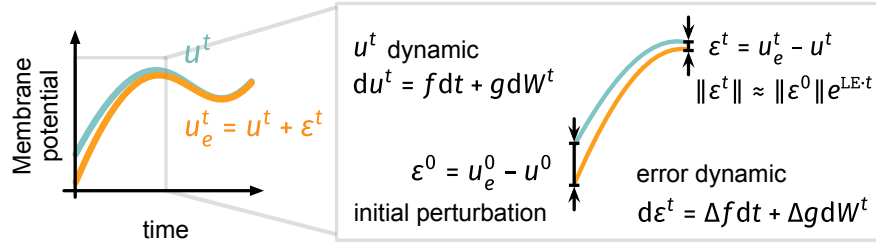


Figure 6: **Illustration of the theoretical analysis.** We study the stability of continuous NSNN sub-threshold dynamic (Equation 20) given a small initial perturbation  $\epsilon^0$  by analyzing the stability of the error dynamic (Equation 22). If the trivial solution  $\epsilon^t = 0$  (with LE being the sample Lyapunov exponent) of the error dynamic is stable, the NSNN system can self-correct small perturbations, keeping the membrane potential in a controllable range and thus producing stable outputs.

be reduced as the system evolves. This means that the system described by Equation 20 is self-correcting and can function reliably in the face of small perturbations or errors. Specifically, we focus on the *almost sure exponential stability* defined as follows.

**Almost sure exponential stability**<sup>95</sup>. The trivial solution  $\epsilon^t = 0$  is *almost surely exponentially stable* if the sample Lyapunov exponent  $LE \triangleq \limsup_{t \rightarrow \infty} \frac{1}{t} \log \|\epsilon^t\|$  is almost surely negative for all  $\epsilon^0 \in \mathbb{R}^{\dim(u^t)}$ .

With LE being the sample Lyapunov exponent of the trivial solution, there exists a positive constant  $C$  and a random variable  $\tau \in [0, \infty)$  such that for all  $t > \tau$ ,  $\|\epsilon^t\| \leq C \exp(t \cdot LE)$  with probability 1. Therefore, the almost sure exponential stability implies that almost all sample paths starting from non-zero initializations will tend to the equilibrium position  $\epsilon^t = 0$  exponentially fast, i.e., the NSNN system can quickly self-correct small perturbations. Further, we have an important result regarding the bounds of the sample Lyapunov exponent as follows.

**Theorem 1** (Bounds for sample Lyapunov exponent of the trivial solution  $\epsilon^t = 0$ ). Suppose that  $0 \leq a_2 \|\epsilon^t\| \leq \|\Delta g(\epsilon^t)\|_F \leq (a_2 + b_2) \|\epsilon^t\|$  for all non-zero  $\epsilon^t \in \mathbb{R}^{\dim(u^t)}$ ,  $t \in \mathbb{R}^+$ . Then, almost surely,

$$a_1 - \frac{1}{2}a_2^2 - b_2^2 - 2a_2b_2 \leq LE \leq a_1 - \frac{1}{2}a_2^2 + \frac{1}{2}b_2^2 + a_2b_2$$

for all  $\epsilon^0 \in \mathbb{R}^{\dim(u^t)}$ .

To prove Theorem 1, we first introduce the differential operator  $L$ . And for the brevity of notations, we temporally omit the superscript  $t$ , viz., we use  $u, \epsilon$  rather than  $u^t, \epsilon^t$  here. The differential operator associated with Equation 22 is defined by

$$L = \frac{\partial}{\partial t} + \sum_{i=1}^{\dim(u)} \Delta f_i(\epsilon, t) \frac{\partial}{\partial \epsilon_i} + \frac{1}{2} \sum_{i,j=1}^{\dim(u)} [\Delta g^\top(\epsilon, t) \Delta g(\epsilon, t)]_{ij} \frac{\partial^2}{\partial \epsilon_i \partial \epsilon_j}, \quad (24)$$

where the subscripts denote the entries of tensors. We also introduce a lemma as follows:

**Lemma 1** (Stochastic Lyapunov theorem). Assume that there exists a non-negative real valued function  $V(\epsilon, t)$  defined on  $\mathbb{R}^{\dim(u)} \times \mathbb{R}^+$ , denoted as  $V \in C^{2,1}(\dim(u) \times \mathbb{R}^+; \mathbb{R}^+)$ . The function  $V$  has continuous partial derivatives denoted as

$$V_\epsilon = \frac{\partial V}{\partial \epsilon}, V_t = \frac{\partial V}{\partial t}, V_{\epsilon, \epsilon} = \frac{\partial^2 V}{\partial \epsilon \partial \epsilon^\top},$$

and constants  $c_1, C_1 > 0$ ,  $c_2, C_2 \in \mathbb{R}$ ,  $c_3, C_3 \geq 0$  such that for all non-zero  $\epsilon$  and  $t \in \mathbb{R}^+$ ,

$$1. \quad c_1 \|\epsilon\|^2 \leq V(\epsilon, t) \leq C_1 \|\epsilon\|^2,$$

2.  $c_2 V(\boldsymbol{\varepsilon}, t) \leq LV(\boldsymbol{\varepsilon}, t) \leq C_2 V(\boldsymbol{\varepsilon}, t),$
3.  $c_3 V(\boldsymbol{\varepsilon}, t)^2 \leq \|V_{\varepsilon}(\boldsymbol{\varepsilon}, t) \Delta \mathbf{g}(\boldsymbol{\varepsilon})\|_F^2 \leq C_3 V(\boldsymbol{\varepsilon}, t)^2.$

Then, the sample Lyapunov exponent satisfies

$$\frac{c_2}{2} - \frac{C_3}{4} \leq \limsup_{t \rightarrow \infty} \frac{1}{t} \log \|\boldsymbol{\varepsilon}\| \leq \frac{C_2}{2} - \frac{c_3}{4} \quad \text{a.s.}$$

Note that this Lemma can be proved by combining Theorems 3.3 and 3.5 in ref.<sup>95</sup> Chapter 4 with  $p = 2$  as in ref.<sup>26</sup>. With Lemma 1 in tow, we then prove Theorem 1.

**Proof** Let  $V(\boldsymbol{\varepsilon}, t) = \|\boldsymbol{\varepsilon}\|^2$ . If we assign  $c_1 = C_1 = 1$ , condition 1 in Lemma 1 is satisfied. By Equation 24, we have

$$LV(\boldsymbol{\varepsilon}, t) = V_{\varepsilon}^{\top} \Delta \mathbf{f}(\boldsymbol{\varepsilon}, t) + \frac{1}{2} \text{trace}(\Delta \mathbf{g}^{\top}(\boldsymbol{\varepsilon}, t) V_{\varepsilon, \varepsilon} \Delta \mathbf{g}(\boldsymbol{\varepsilon}, t)),$$

Then, by Equations 21, 22, we can easily show that for all non-zero  $\boldsymbol{\varepsilon} \in \mathbb{R}^{\dim(u)}$ ,  $t \in \mathbb{R}^+$ ,

$$(2a_1 + a_2^2) \|\boldsymbol{\varepsilon}\|^2 \leq LV(\boldsymbol{\varepsilon}, t) \leq (2a_1 + (a_2 + b_2)^2) \|\boldsymbol{\varepsilon}\|^2.$$

Hence, condition 2 in Lemma 1 is satisfied.

To satisfy the condition 3 in Lemma 1, by the assumption on  $\Delta \mathbf{g}$ , we have

$$4a_2^2 V^2 \leq \|V_{\varepsilon} \Delta \mathbf{g}\|_F^2 \leq 4(a_2 + b_2)^2 V^2.$$

In conclusion, let  $c_1 = 1, C_1 = 1, c_2 = 2a_1 + a_2^2, C_2 = 2a_1 + (a_2 + b_2)^2, c_3 = 4a_2^2, C_3 = 4(a_2 + b_2)^2$ , we obtain the bounds of the sample Lyapunov exponent by Lemma 1, that is

$$a_1 - \frac{1}{2}a_2^2 - b_2^2 - 2a_2b_2 \leq \text{LE} \leq a_1 - \frac{1}{2}a_2^2 + \frac{1}{2}b_2^2 + a_2b_2.$$

Q.E.D.

According to Theorem 1, the lower bound LB and upper bound UB of the sample Lyapunov exponent of the trivial solution  $\boldsymbol{\varepsilon}^t = 0$  is

$$LB = a_1 - \frac{1}{2}a_2^2 - b_2^2 - 2a_2b_2, \quad UB = a_1 - \frac{1}{2}a_2^2 + \frac{1}{2}b_2^2 + a_2b_2.$$

Generally, by the definition of almost sure exponential stability, if  $UB < 0$ , the trivial solution is almost sure exponentially stable. And even if  $a_1 > 0$ , the system can still be stabilized by introducing internal noise terms to ensure a negative upper bound. For LIF-modeling spiking neural nets, as  $a_1 = -\frac{1}{\tau_m} < 0$ , if  $\frac{1}{\tau_m} > -\frac{1}{2}a_2^2 + \frac{1}{2}b_2^2 + a_2b_2$ , then we have that the sub-threshold dynamic system is self-correcting, i.e.,  $\boldsymbol{\varepsilon}^t \xrightarrow{\text{a.s.}} 0$ . We then turn to the special case when the noise is additive ( $a_2 > 0, b_2 \rightarrow 0$ ). NSNNs introduced in this article belong to this category. In the additive noise case, the multiplicative noise component in the system tends to zero  $b_2 \rightarrow 0$ , and the upper bound of the sample Lyapunov exponent becomes  $UB_{\text{additive}} = a_1 - \frac{1}{2}a_2^2$ . On the other hand, in the noiseless case, both noise terms tend to zero,  $a_2 \rightarrow 0, b_2 \rightarrow 0$ , and the lower bound is  $LB_{\text{noise free}} = a_1$ . Therefore we have that  $UB_{\text{additive}} < LB_{\text{noise free}} = a_1 < 0$ . In a small time interval, for the error at time  $t$ , we have  $\|\boldsymbol{\varepsilon}^t\| = \|\boldsymbol{\varepsilon}^0\| \exp(\text{LE} \cdot t)$ . Therefore, introducing additive noise ensures a more negative Lyapunov exponent than in the noiseless case, resulting in faster self-correction. This allows rapid detection and correction of factors that may cause instability, thereby improving NSNN system stability.



## Experimental details

Experiments were conducted using a workstation with an Intel I5-10400, 64 GB RAM, and two NVIDIA RTX 3090. The results are reported as mean and SD across independent runs.

### Details of recognition experiments

The CIFAR dataset<sup>59</sup> includes 50k  $32 \times 32$  images for training and 10k for evaluation. We adopt random crop, random horizontal flip, and AutoAugment<sup>96</sup> for the training samples. The preprocessed samples are normalized using z-score scaling in the training and evaluation phases. The DVS-CIFAR dataset<sup>60</sup> is a challenging neuromorphic benchmark recorded via a DVS camera using images from CIFAR-10. We adopt pre-processing pipeline in previous works<sup>97</sup>, i.e., divide the original set into a 9k-sample training set and 1k-sample evaluation set, and all event stream files are spatially downsampled to  $48 \times 48$ . We augment the training samples following previous studies<sup>9</sup>. The DVS-Gesture dataset<sup>61</sup> is recorded using a DVS128 event camera. It contains recordings of 11 hand gestures from 29 subjects under three illumination conditions.

We optimized SNN models using the dataset’s observation-label pairs and calculated performance metrics on non-overlapping test data. Prediction accuracy was used as the performance metric for these tasks. For each network architecture and SNN algorithm combination, we set the optimal hyperparameters for DSNNs and NSNNs under different architecture and algorithm combinations via grid search to ensure a fair comparison. We indicate the corresponding simulation timestep in the results, which is the simulation duration of our discrete SNN implementation. The static image is repeatedly inputted for static image data, so a longer simulation timestep usually results in more accurate recognition. For event stream datasets, the fixed-length continuous event streams were discretized into simulation timestep time windows. Hence, a larger simulation timestep leads to more refined computation and more accurate recognition.

We set the standard deviation of membrane noise to 0.3 for CIFAR-10, CIFAR-100, and DVS-Gesture experiments and 0.2 for DVS-CIFAR ones. These configurations offer a fair balance between performance and resilience. For the SGL of DSNNs, we employ the ERF surrogate gradient  $\text{SG}_{\text{ERF}}(x) = \frac{1}{\sqrt{\pi}} \exp(-x^2)$ . Adam solvers<sup>98</sup> with the cosine annealing learning rate scheduler<sup>99</sup> was used to train all networks. We list hyper-parameters we adopted in recognition experiments in Table 4. The initial learning rate is obtained through a grid search. The ResNet-19<sup>100</sup>, VGGSNN<sup>9</sup>, CIFAR-Net<sup>8</sup>, and 7B-Net<sup>101</sup> SNN architectures used in this article follow the original implementation in previous works. The ResNet-18 architecture is given by 64C3-2(64C3-4C3)-2(128C3-128C3)-2(256C3-256C3)-2(512C3-512C3)-AP-FC. AP denotes average pooling, FC denotes the fully connected layer, and C denotes the convolution layer. The SNN algorithms STBP<sup>7</sup>, STBP-ttBN<sup>100</sup> (ttBN), and TET<sup>9</sup> used here also follow the original implementations presented in previous literature.

Here, we also visualize representative learning curves of DSNNs and NSNNs. As seen from Figure 7, NSNNs demonstrated higher learning efficiency than DSNNs. And this advantage is more pronounced on datasets prone to overfitting, such as the DVS-CIFAR data. We also noticed that using NSNNs results in a slight increase in training time compared to DSNNs. This is mainly because the firing process in Noisy LIF neurons involves computing the firing probability and then sampling from the Bernoulli distribution. Much of this additional time comes from the sampling step since the PyTorch framework we use has no targeted optimizations for sampling from random distributions. For instance, training a CIFARNet on CIFAR-10 data takes about 183 minutes for DSNNs and 194 minutes for NSNNs.

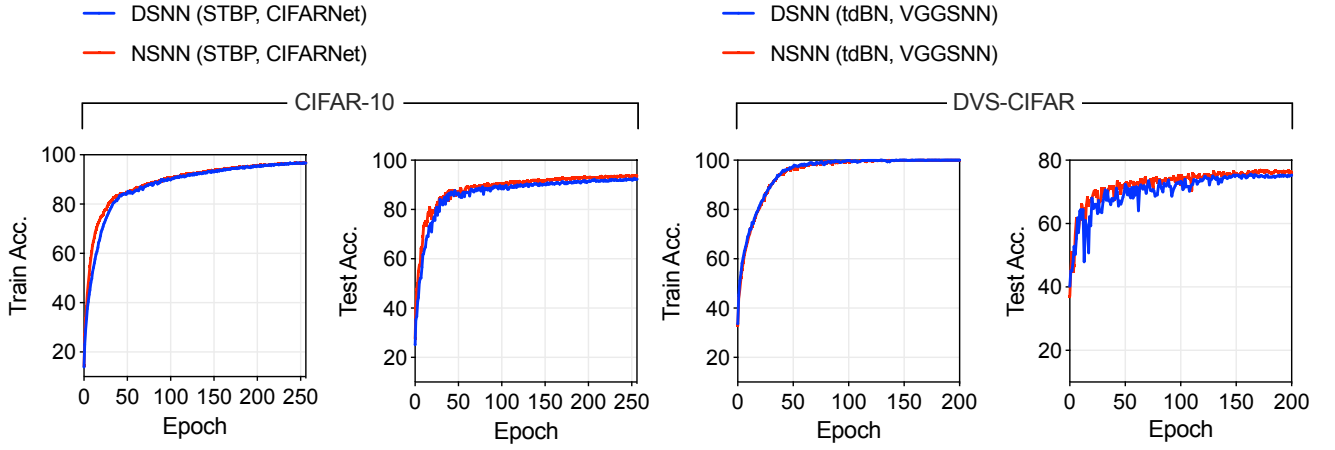


Figure 7: **Example learning curves on CIFAR-10 and DVS-CIFAR.**

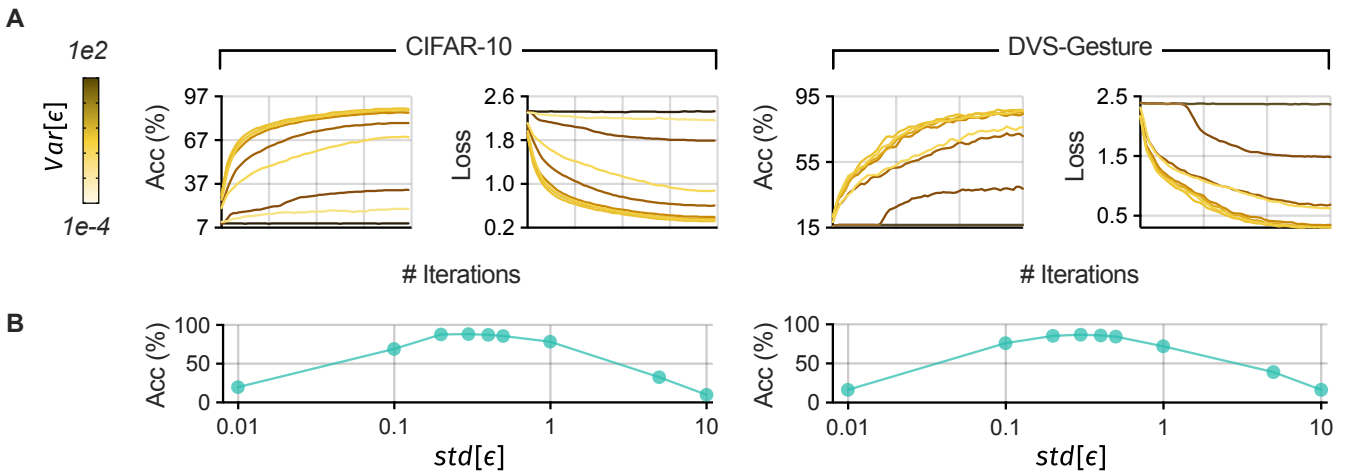


Figure 8: **Effect of internal noise level on performance.** **A** Learning curves of NSNNs under different noise levels, we use color to distinguish different noise levels. **B** The relationship between final test accuracy and the standard deviation of internal noise  $\epsilon$ .

### Effect of internal noise level on network performance

The internal noise level influences learning as the post-synaptic factor  $F'_\epsilon(u - v_{th})$  in NDL is calculated using the probability density function of membrane noise  $\epsilon$ . When the variance is tiny, the noise distribution converges to a Dirac distribution with limited information (as measured by information entropy), preventing the post-synaptic factor from obtaining enough information to perform learning effectively. In the case of inference, the noise level directly influences the randomness of the firing distribution. A high variance noise would disrupt the flow of decisive information in the network, leading to greatly deteriorated performance.

We have provided a theoretical explanation regarding internal noise, network stability, and performance in the previous content. Here we show empirically that mild noise is beneficial for network performance. Our empirical findings are consistent with previous literature<sup>62</sup> that suggests a certain amount of noise can improve network performance. We ran experiments using the CIFAR-10 and DVS-Gesture datasets and trained identical networks with different internal noise level settings for 60 epochs. Results are presented by learning curves and the accuracy-standard deviation curves in Figure 8A. Our observations show that when the variance of internal noise increases from 0, the model's performance initially improves and then declines. Notably, NSNNs achieve high performance near a

moderate value (refer to Figure 8B), confirming our intuition that moderate noise is essential for high performance. According to our results, changes in  $\text{std}[\epsilon]$  within a *moderate noise* range (from 0.2 to 0.5) have no significant effect on final performance. This gives us a range of internal noise levels to choose from when using NSNNs in practice.

### Details of recognition experiments with perturbations

Here we list the details of the external perturbations in our experiments as follows. We denote the model to be evaluated as NN. In the Direct Optimization (DO) method, we construct the adversarial samples by directly solving the constrained optimization problem

$$\Delta x = \operatorname{argmax}_{\|\Delta x\|_2=\gamma} \text{loss}(f(x + \Delta x), y), \quad (25)$$

where  $\Delta x$  for the adversarial perturbation and  $x + \Delta x$  is the adversarial example. It is implemented using PyTorch and GeoTorch<sup>102</sup> toolkits. The L-2 norm bounded additive disturbance tensors are zero-initialized and optimized by an Adam solver with a learning rate of 0.002 for 30 iterations. After that, the additive perturbations are used to produce adversarial samples and fed into the target models (DSNNs or NSNNs in this work). The implementation of the FGSM method follows the original implementation<sup>103</sup>, where the adversarial example is constructed as

$$\tilde{x}^{adv} = x + \gamma_{FGSM} \times \text{sign}[\nabla_x \text{loss}(\text{NN}(x), y)]. \quad (26)$$

The input-level EventDrop<sup>64</sup> perturbation for dynamic inputs is constructed by randomly dropping spikes in the raw input spike trains. The dropping probability is set by a parameter  $\rho$ . The strategy of dropping we consider is Random Drop<sup>64</sup>, which combines spatial and temporal-wise event-dropping strategies. During the evaluation, we first individually performed EventDrop over every sample from the test set and then fed our testees with the disturbed inputs.

The spike state-level perturbation includes two disturbances: the emission state from 1 to 0 (spike to silence) and the emission state from 0 to 1 (silence to spike). To simplify the settings, we use one parameter  $\beta$  to control the probability of both kinds of changes. Let variable  $o_{old}$  denotes the original spike state, if  $o_{old} = 1$ , we have  $\mathbb{P}[o_{new} = 0] = \beta$ , else, if  $o_{old} = 0$ ,  $\mathbb{P}[o_{new} = 1] = \beta$ .

### Details of recognition task coding analyses

In this part, we used the learned models in previous recognition experiments; their simulation timesteps are 2, 2, 10, and 16, respectively. The number of test samples for computing the Pearson correlation coefficients is 500 for CIFAR-10, CIFAR-100, DVS-CIFAR, and 200 for DVS-Gesture.

The Fano factor<sup>104</sup> measures the spike count variability. Let us denote the spike count of neuron  $(L, m)$  as  $n_{L,m}^{\text{trial ID}}$ , the average value as  $\bar{n}_{L,m} = \frac{1}{\# \text{ trials}} \sum_k n_{L,m}^k$ . The deviations from the mean is computed as  $\Delta n_{L,m}^{\text{trial ID}} = n_{L,m}^{\text{trial ID}} - \bar{n}_{L,m}$ , and the Fano factor is  $\text{FF}_{L,m} = \frac{\text{Var}[n_{L,m}]}{\bar{n}_{L,m}}$ .

### Details of neural activity fitting experiments

In the neural activity fitting experiment, we used neural recordings of dark-adapted axolotl salamander retinas<sup>68</sup>. The original dataset contains the retinal neural responses of two retinas to two movies. We only used a part of the data (retina 2 with movie 2) in this experiment. It contains complex natural scenes of a tiger on a prey hunt, roughly 60 s long. The movie was discretized into bins of 33 ms, and all frames were converted to grayscale with a resolution of 360 pixel×360 pixel at 7.5  $\mu\text{m}$ ×7.5  $\mu\text{m}$  per pixel, covering a 2700  $\mu\text{m}$ ×2700  $\mu\text{m}$  area on the retina. The neural recording contains 42 repetitions of 49 cells. We partitioned all records into stimuli-response sample pairs of 1 second and down-sampled the frames to 90 pixel×90 pixel. The data was split into non-overlapping train/test (50%/50%) parts.

In the neural activity fitting experiment, the network architecture for the DSNN and NSNN models is 16C25-32C11-FC64-FC64-FC64-FC49. FC denotes the fully connected layer, and C denotes the convolutional layer. These models were trained using the Adam optimizer with a cosine-decay learning rate scheduler, starting at a rate of 0.0003. The mini-batch size was set to 64, and the models were trained for 64 epochs. At test time, the test samples have the same length as the training samples (1 second) by default. During training, the DSNN and NSNN models are optimized to minimize the Maximum Mean Discrepancy (MMD) loss<sup>105,106</sup>. We use the first-order postsynaptic potential (PSP) kernel<sup>107</sup> that can effectively depict the temporal dependencies in spike train data. Denoting the predicted, recorded spike trains as  $\hat{\mathbf{y}}, \mathbf{y}$ , respectively, we can write the PSP kernel MMD predictive loss as

$$\mathcal{L}_{\text{PSP-MMD}} = \frac{1}{T} \sum_{t=1}^T \sum_{\tau=1}^t \left\| \text{PSP}(\hat{\mathbf{y}}_{1:\tau}) - \text{PSP}(\mathbf{y}_{1:\tau}) \right\|^2, \quad (27)$$

where  $\text{PSP}(\mathbf{y}_{1:\tau}) = (1 - \frac{1}{\tau_s})\text{PSP}(\mathbf{y}_{1:\tau-1}) + \frac{1}{\tau_s}\mathbf{y}_\tau$ , and we set the time constant  $\tau_s = 2$ . For the DSNN model, we used the ERF surrogate gradient as in the recognition experiments. And for the NSNN model, the internal noise is  $\mathcal{N}(0, 0.2^2)$ .

The CNN baseline we used adopts the architecture: 32C25-BN-16C11-BN-FC49-BN-PSoftPlus, where BN denotes the Batch-Normalization operation, and PSoftPlus denotes the parameterized SoftPlus activation. The training specifications follow the implementation in the previous work<sup>69</sup>.

## Acknowledgments

Use this section to acknowledge contributions from non-authors and list funding sources, including grant numbers.

## Author contributions

This section is required for all research papers.

## Declaration of interests

The authors declare no competing interests.

## Tables, table titles, and table legends

Table 1: **Evaluation results on CIFAR-10, CIFAR-100, DVS-CIFAR and DVS-Gesture datasets.**

NSNN	SNN algorithm	SNN architecture	Accuracy	Accuracy
<b>CIFAR-10:</b>				
			<b>timestep=2</b>	<b>timestep=4</b>
	STCA	CIFARNet	91.23 (timestep=12)	
	STBP-tdBN	ResNet-19	92.34	92.92
	STBP	ResNet-18	93.18 $\pm$ 0.07	93.93 $\pm$ 0.11
Yes	STBP	ResNet-18	92.87 $\pm$ 0.04	93.77 $\pm$ 0.12
	STBP	CIFARNet	91.88 $\pm$ 0.09	92.79 $\pm$ 0.14
Yes	STBP	CIFARNet	93.90 $\pm$ 0.12	94.30 $\pm$ 0.08
	TET	ResNet-18	93.62 $\pm$ 0.02	94.09 $\pm$ 0.20
Yes	TET	ResNet-18	93.12 $\pm$ 0.07	94.14 $\pm$ 0.05
<b>CIFAR-100:</b>				
			<b>timestep=2</b>	<b>timestep=4</b>
	TET	ResNet-19	72.87 $\pm$ 0.10	74.47 $\pm$ 0.15
	STBP-tdBN	ResNet-19	69.41 $\pm$ 0.08	70.86 $\pm$ 0.22
	STBP	ResNet-18	70.15 $\pm$ 0.14	70.88 $\pm$ 0.19
Yes	STBP	ResNet-18	69.57 $\pm$ 0.09	71.16 $\pm$ 0.40
	STBP	CIFARNet	72.25 $\pm$ 0.08	72.94 $\pm$ 0.21
Yes	STBP	CIFARNet	73.36 $\pm$ 0.14	74.17 $\pm$ 0.28
	TET	ResNet-18	71.72 $\pm$ 0.13	74.01 $\pm$ 0.43
Yes	TET	ResNet-18	71.34 $\pm$ 0.09	73.33 $\pm$ 0.03
<b>DVS-CIFAR:</b>				
			<b>timestep=10</b>	
	Fang et al.	Wide-7B-Net	74.40 (timestep=16)	
	Wu et al.	LIAFNet	71.70	
	STBP	ResNet-19	71.74 $\pm$ 0.92	
Yes	STBP	ResNet-19	74.30 $\pm$ 0.61	
	STBP-tdBN	VGGSNN	75.51 $\pm$ 0.49	
Yes	STBP-tdBN	VGGSNN	76.97 $\pm$ 0.10	
	TET	VGGSNN	78.26 $\pm$ 0.17	
Yes	TET	VGGSNN	79.52 $\pm$ 0.38	
<b>DVS-Gesture:</b>				
			<b>timestep=16</b>	
	Fang et al.	7B-Net	97.92	
	STBP-tdBN	ResNet-17	96.87 (timestep=40)	
	STBP	7B-Net	95.84 $\pm$ 0.27	
Yes	STBP	7B-Net	96.88 $\pm$ 0.28	

Table 2: **Evaluation results under EventDrop input-level perturbation on DVS-CIFAR data.** Larger  $\rho$  denotes stronger perturbation. The results show that NSNNs are more robust to challenging input perturbations.

Algorithm & Architecture	NSNN	$\rho=0.05$	$\rho=0.25$	$\rho=0.45$	$\rho=0.65$
Loss					
STBP &		2.27 $\pm$ 0.16	6.89 $\pm$ 2.05	8.60 $\pm$ 1.55	9.06 $\pm$ 1.08
ResNet-19	Yes	1.80 $\pm$ 0.09	5.84 $\pm$ 0.76	7.65 $\pm$ 1.21	8.55 $\pm$ 1.40
tdBN &		2.24 $\pm$ 0.14	6.31 $\pm$ 0.74	8.25 $\pm$ 1.49	9.49 $\pm$ 1.61
VGGSNN	Yes	1.90 $\pm$ 0.06	6.91 $\pm$ 0.16	8.19 $\pm$ 0.82	8.66 $\pm$ 1.35
TET &		1.21 $\pm$ 0.01	2.88 $\pm$ 0.31	3.44 $\pm$ 0.31	4.13 $\pm$ 0.57
VGGSNN	Yes	1.03 $\pm$ 0.05	2.55 $\pm$ 0.25	4.02 $\pm$ 0.29	4.15 $\pm$ 0.18
Accuracy (%)					
STBP &		60.09 $\pm$ 2.46	17.68 $\pm$ 5.72	13.21 $\pm$ 1.31	12.42 $\pm$ 0.29
ResNet-19	Yes	65.66 $\pm$ 1.80	25.31 $\pm$ 5.72	16.36 $\pm$ 3.23	13.32 $\pm$ 0.61
tdBN &		64.98 $\pm$ 1.63	26.64 $\pm$ 3.32	18.41 $\pm$ 2.43	13.74 $\pm$ 1.00
VGGSNN	Yes	70.28 $\pm$ 1.36	30.14 $\pm$ 0.99	22.55 $\pm$ 2.07	18.78 $\pm$ 1.97
TET &		67.86 $\pm$ 0.43	29.26 $\pm$ 4.34	20.76 $\pm$ 2.45	15.70 $\pm$ 2.80
VGGSNN	Yes	71.67 $\pm$ 1.20	29.14 $\pm$ 1.16	21.34 $\pm$ 0.73	14.73 $\pm$ 0.29

Table 3: **Evaluation results under spike state-level (firing state of spiking neurons) perturbation on DVS-CIFAR data.** Larger  $\beta$  denotes stronger perturbation. The results show that NSNNs are more robust to challenging spike state perturbations.

Algorithm & Architecture	NSNN	$\beta=0.01$	$\beta=0.02$	$\beta=0.03$	$\beta=0.04$
Loss					
STBP & ResNet-19		1.43 $\pm$ 0.04	1.72 $\pm$ 0.06	2.44 $\pm$ 0.03	3.43 $\pm$ 0.25
	Yes	1.23 $\pm$ 0.04	1.30 $\pm$ 0.03	1.41 $\pm$ 0.13	1.74 $\pm$ 0.32
tdBN & VGGSNN		1.29 $\pm$ 0.05	1.30 $\pm$ 0.08	1.49 $\pm$ 0.18	1.88 $\pm$ 0.29
	Yes	1.25 $\pm$ 0.01	1.19 $\pm$ 0.02	1.22 $\pm$ 0.06	1.50 $\pm$ 0.13
TET & VGGSNN		0.82 $\pm$ 0.03	0.91 $\pm$ 0.06	1.08 $\pm$ 0.08	1.37 $\pm$ 0.06
	Yes	0.75 $\pm$ 0.01	0.80 $\pm$ 0.01	0.94 $\pm$ 0.06	1.25 $\pm$ 0.14
Accuracy (%)					
STBP & ResNet-19		69.73 $\pm$ 0.88	63.91 $\pm$ 1.37	53.60 $\pm$ 1.39	40.32 $\pm$ 1.91
	Yes	72.88 $\pm$ 0.69	70.44 $\pm$ 0.42	67.27 $\pm$ 2.66	58.99 $\pm$ 6.80
tdBN & VGGSNN		74.09 $\pm$ 0.66	70.61 $\pm$ 1.37	63.19 $\pm$ 2.89	50.74 $\pm$ 3.32
	Yes	76.16 $\pm$ 0.13	73.38 $\pm$ 0.55	68.77 $\pm$ 0.78	55.64 $\pm$ 1.87
TET & VGGSNN		76.41 $\pm$ 0.92	72.60 $\pm$ 1.11	66.46 $\pm$ 1.93	56.06 $\pm$ 1.05
	Yes	78.28 $\pm$ 0.27	76.32 $\pm$ 1.01	71.54 $\pm$ 1.07	62.48 $\pm$ 0.52



Table 4: **Hyper-parameter settings for recognition experiments.**

<b>NSNN</b>	<b>Data</b>	<b>SNN algorithm</b>	<b>SNN architecture</b>	<b>Simulation timestep</b>	<b>Initial learning rate</b>	<b>Mini-batch size</b>
	CIFAR-10	STBP	ResNet-18	2/4	0.01	256/256
	CIFAR-10	TET	ResNet-18	2/4	0.01	256/256
	CIFAR-10	STBP	CIFARNet	2/4	0.004	256/256
	CIFAR-100	STBP	ResNet-18	2/4	0.005	256/256
	CIFAR-100	TET	ResNet-18	2/4	0.005	256/256
	CIFAR-100	STBP	CIFARNet	2/4	0.001	256/256
	DVS-CIFAR	STBP	ResNet-19	10	0.0005	32
	DVS-CIFAR	TET	VGGSNN	10	0.0002	64
	DVS-CIFAR	tdBN	VGGSNN	10	0.0002	64
	DVS-Gesture	STBP	7B-Net	16	0.001	10
Yes	CIFAR-10	STBP	ResNet-18	2/4	0.002	256/256
Yes	CIFAR-10	TET	ResNet-18	2/4	0.002	256/256
Yes	CIFAR-10	STBP	CIFARNet	2/4	0.003	256/128
Yes	CIFAR-100	STBP	ResNet-18	2/4	0.001	256/256
Yes	CIFAR-100	TET	ResNet-18	2/4	0.001	256/256
Yes	CIFAR-100	STBP	CIFARNet	2/4	0.002	256/128
Yes	DVS-CIFAR	STBP	ResNet-19	10	0.0005	20
Yes	DVS-CIFAR	TET	VGGSNN	10	0.0003	32
Yes	DVS-CIFAR	tdBN	VGGSNN	10	0.0003	32
Yes	DVS-Gesture	STBP	7B-Net	16	0.0005	8

## References

1. Zilli, E. A., and Hasselmo, M. E. (2010). Coupled noisy spiking neurons as velocity-controlled oscillators in a model of grid cell spatial firing. *Journal of Neuroscience* 30, 13850–13860.
2. Teeter, C., Iyer, R., Menon, V., Gouwens, N., Feng, D., Berg, J., Szafer, A., Cain, N., Zeng, H., Hawrylycz, M. et al. (2018). Generalized leaky integrate-and-fire models classify multiple neuron types. *Nature communications* 9, 709.
3. Simonyan, K., and Zisserman, A. (2014). Very deep convolutional networks for large-scale image recognition. *arXiv*.
4. Szegedy, C., Liu, W., Jia, Y., Sermanet, P., Reed, S., Anguelov, D., Erhan, D., Vanhoucke, V., and Rabinovich, A. Going deeper with convolutions. In: *CVPR* (2015):( 1–9).
5. He, K., Zhang, X., Ren, S., and Sun, J. Deep residual learning for image recognition. In: *CVPR* (2016):( 770–778).
6. Lee, J. H., Delbruck, T., and Pfeiffer, M. (2016). Training deep spiking neural networks using backpropagation. *Frontiers in Neuroscience* 10.
7. Wu, Y., Deng, L., Li, G., Zhu, J., and Shi, L. (2018). Spatio-temporal backpropagation for training high-performance spiking neural networks. *Frontiers in Neuroscience* 12, 1–12.
8. Wu, Y., Deng, L., Li, G., Zhu, J., Xie, Y., and Shi, L. Direct training for spiking neural networks: Faster, larger, better. In: *Proceedings of the AAAI conference on artificial intelligence* (2019):.
9. Deng, S., Li, Y., Zhang, S., and Gu, S. Temporal efficient training of spiking neural network via gradient re-weighting. In: *International Conference on Learning Representations* (2021):.
10. Shen, G., Zhao, D., and Zeng, Y. (2022). Backpropagation with biologically plausible spatiotemporal adjustment for training deep spiking neural networks. *Patterns* 3, 100522.
11. Volinski, A., Zaidel, Y., Shalumov, A., DeWolf, T., Supic, L., and Tsur, E. E. (2022). Data-driven artificial and spiking neural networks for inverse kinematics in neurorobotics. *Patterns* 3, 100391.
12. Zhao, F., Zeng, Y., Han, B., Fang, H., and Zhao, Z. (2022). Nature-inspired self-organizing collision avoidance for drone swarm based on reward-modulated spiking neural network. *Patterns* 3, 100611.
13. Fang, W., Yu, Z., Chen, Y., Huang, T., Masquelier, T., and Tian, Y. Deep residual learning in spiking neural networks. In: *Advances in Neural Information Processing Systems (NeurIPS)* (2021):.
14. Liu, Q., Ruan, H., Xing, D., Tang, H., and Pan, G. Effective aer object classification using segmented probability-maximization learning in spiking neural networks. In: *Proceedings of the AAAI conference on artificial intelligence* (2020):.
15. Roy, K., Jaiswal, A., and Panda, P. (2019). Towards spike-based machine intelligence with neuromorphic computing. *Nature* 575, 607–617.
16. Verveen, A., and DeFelice, L. (1974). Membrane noise. *Progress in Biophysics and Molecular Biology* 28, 189–265.

17. Kempter, R., Gerstner, W., Van Hemmen, J. L., and Wagner, H. (1998). Extracting oscillations: Neuronal coincidence detection with noisy periodic spike input. *Neural computation* 10, 1987–2017.
18. Stein, R. B. (1965). A theoretical analysis of neuronal variability. *Biophysical Journal* 5, 173–194.
19. Stein, R. B., Gossen, E. R., and Jones, K. E. (2005). Neuronal variability: noise or part of the signal? *Nature Reviews Neuroscience* 6, 389–397.
20. Faisal, A. A., Selen, L. P., and Wolpert, D. M. (2008). Noise in the nervous system. *Nature Reviews Neuroscience* 9, 292–303.
21. Maass, W. On the computational power of noisy spiking neurons. In: *Advances in Neural Information Processing Systems (NeurIPS)* (1995):.
22. Maass, W. Noisy spiking neurons with temporal coding have more computational power than sigmoidal neurons. In: *Advances in Neural Information Processing Systems (NeurIPS)* (1996):.
23. Patel, A., and Kosko, B. (2005). Stochastic resonance in noisy spiking retinal and sensory neuron models. *Neural Networks* 18, 467–478.
24. Liu, X., Xiao, T., Si, S., Cao, Q., Kumar, S., and Hsieh, C.-J. How does noise help robustness? explanation and exploration under the neural sde framework. In: *CVPR* (2020): ( 282–290).
25. Camuto, A., Willetts, M., Simsekli, U., Roberts, S. J., and Holmes, C. C. Explicit regularisation in gaussian noise injections. In: *Advances in Neural Information Processing Systems (NeurIPS)* vol. 33 (2020): ( 16603–16614).
26. Lim, S. H., Erichson, N. B., Hodgkinson, L., and Mahoney, M. W. Noisy recurrent neural networks. In: *Advances in Neural Information Processing Systems (NeurIPS)* (2021):.
27. Hinton, G. E., Srivastava, N., Krizhevsky, A., Sutskever, I., and Salakhutdinov, R. R. (2012). Improving neural networks by preventing co-adaptation of feature detectors. *arXiv*.
28. Gerstein, G. L., and Mandelbrot, B. (1964). Random walk models for the spike activity of a single neuron. *Biophysical Journal* 4, 41–68.
29. Tuckwell, H. C. *Stochastic Processes in the Neurosciences*. SIAM (1989).
30. Plesser, H. E., and Gerstner, W. (2000). Noise in integrate-and-fire neurons: from stochastic input to escape rates. *Neural Computation* 12, 367–384.
31. Gerstner, W., Kistler, W. M., Naud, R., and Paninski, L. *Neuronal dynamics: From single neurons to networks and models of cognition*. Cambridge University Press (2014).
32. Rao, R. P. (2004). Bayesian computation in recurrent neural circuits. *Neural Computation* 16, 1–38.
33. Rao, R. P. Hierarchical bayesian inference in networks of spiking neurons. In: *Advances in Neural Information Processing Systems (NeurIPS)* vol. 17 (2004):.
34. Deneve, S. Bayesian inference in spiking neurons. In: *Advances in Neural Information Processing Systems (NeurIPS)* vol. 17 (2004):.

35. Kasabov, N. (2010). To spike or not to spike: A probabilistic spiking neuron model. *Neural Networks* 23, 16–19.
36. Skatchkovsky, N., Jang, H., and Simeone, O. (2021). Spiking neural networks—part ii: Detecting spatio-temporal patterns. *IEEE Communications Letters* 25, 1741–1745.
37. Neftci, E. O., Mostafa, H., and Zenke, F. (2019). Surrogate gradient learning in spiking neural networks: Bringing the power of gradient-based optimization to spiking neural networks. *IEEE Signal Processing Magazine* 36, 51–63.
38. Cramer, B., Billaudelle, S., Kanya, S., Leibfried, A., Grübl, A., Karasenko, V., Pehle, C., Schreiber, K., Stradmann, Y., Weis, J., Schemmel, J., and Zenke, F. (2022). Surrogate gradients for analog neuromorphic computing. *Proceedings of the National Academy of Sciences* 119, e2109194119. doi:10.1073/pnas.2109194119.
39. Eshraghian, J. K., Ward, M., Neftci, E., Wang, X., Lenz, G., Dwivedi, G., Bennamoun, M., Jeong, D. S., and Lu, W. D. (2021). Training spiking neural networks using lessons from deep learning. *arXiv preprint arXiv:2109.12894*.
40. Bellec, G., Scherr, F., Subramoney, A., Hajek, E., Salaj, D., Legenstein, R., and Maass, W. (2020). A solution to the learning dilemma for recurrent networks of spiking neurons. *Nature Communications* 11, 1–15.
41. Rumelhart, D. E., Hinton, G. E., and Williams, R. J. (1986). Learning representations by back-propagating errors. *Nature* 323, 533–536.
42. Zenke, F., and Vogels, T. P. (2021). The remarkable robustness of surrogate gradient learning for instilling complex function in spiking neural networks. *Neural Computation* 33, 899–925.
43. Jang, H., Simeone, O., Gardner, B., and Gruning, A. (2019). An introduction to probabilistic spiking neural networks: Probabilistic models, learning rules, and applications. *IEEE Signal Processing Magazine* 36, 64–77.
44. Dan, Y., and Poo, M.-m. (2004). Spike timing-dependent plasticity of neural circuits. *Neuron* 44, 23–30.
45. Froemke, R. C., Poo, M.-m., and Dan, Y. (2005). Spike-timing-dependent synaptic plasticity depends on dendritic location. *Nature* 434, 221–225.
46. Guyonneau, R., VanRullen, R., and Thorpe, S. J. (2005). Neurons tune to the earliest spikes through stdp. *Neural Computation* 17, 859–879.
47. Maass, W. (2014). Noise as a resource for computation and learning in networks of spiking neurons. *Proceedings of the IEEE* 102, 860–880.
48. Burkitt, A. N. (2006). A review of the integrate-and-fire neuron model: I. homogeneous synaptic input. *Biological Cybernetics* 95, 1–19.
49. Heckerman, D., Geiger, D., and Chickering, D. M. (1995). Learning bayesian networks: The combination of knowledge and statistical data. *Machine learning* 20, 197–243.
50. Heckerman, D. A tutorial on learning with Bayesian networks. Springer (1998).
51. Zenke, F., and Neftci, E. O. (2021). Brain-inspired learning on neuromorphic substrates. *Proceedings of the IEEE* 109, 935–950.

52. Wu, Y., Zhao, R., Zhu, J., Chen, F., Xu, M., Li, G., Song, S., Deng, L., Wang, G., Zheng, H. et al. (2022). Brain-inspired global-local learning incorporated with neuromorphic computing. *Nature Communications* 13, 65.
53. Frémaux, N., and Gerstner, W. (2016). Neuromodulated spike-timing-dependent plasticity, and theory of three-factor learning rules. *Frontiers in Neural Circuits* 9, 85.
54. Gerstner, W., Lehmann, M., Liakoni, V., Corneil, D., and Brea, J. (2018). Eligibility traces and plasticity on behavioral time scales: experimental support of neohebbian three-factor learning rules. *Frontiers in Neural Circuits* 12, 53.
55. Hubara, I., Courbariaux, M., Soudry, D., El-Yaniv, R., and Bengio, Y. Binarized neural networks (2016).
56. Tokui, S., and Sato, I. Evaluating the variance of likelihood-ratio gradient estimators. In: *International Conference on Machine Learning* vol. 7 (2017):( 5244–5257).
57. Hou, L., Yao, Q., and Kwok, J. T. Loss-aware binarization of deep networks. In: *International Conference on Learning Representations* (2017):( 1–11).
58. Yin, P., Lyu, J., Zhang, S., Osher, S., Qi, Y., and Xin, J. Understanding straight-through estimator in training activation quantized neural nets. In: *International Conference on Learning Representations* (2019):( 1–30).
59. Krizhevsky, A., Hinton, G. et al. (2009). Learning multiple layers of features from tiny images.
60. Li, H., Liu, H., Ji, X., Li, G., and Shi, L. (2017). Cifar10-dvs: an event-stream dataset for object classification. *Frontiers in neuroscience* 11, 309.
61. Amir, A., Taba, B., Berg, D., Melano, T., McKinstry, J., Di Nolfo, C., Nayak, T., Andreopoulos, A., Garreau, G., Mendoza, M. et al. A low power, fully event-based gesture recognition system. In: *CVPR* (2017):( 7243–7252).
62. Basalyga, G., and Salinas, E. (2006). When response variability increases neural network robustness to synaptic noise. *Neural Computation* 18, 1349–1379.
63. McDonnell, M. D., and Ward, L. M. (2011). The benefits of noise in neural systems: bridging theory and experiment. *Nature Reviews Neuroscience* 12, 415–425.
64. Gu, F., Sng, W., Hu, X., and Yu, F. (2021). Eventdrop: Data augmentation for event-based learning. *arXiv*.
65. Mainen, Z. F., and Sejnowski, T. J. (1995). Reliability of spike timing in neocortical neurons. *Science* 268, 1503–1506.
66. Tiesinga, P., Fellous, J.-M., and Sejnowski, T. J. (2008). Regulation of spike timing in visual cortical circuits. *Nature reviews neuroscience* 9, 97–107.
67. de Ruyter van Steveninck, R. R., Lewen, G. D., Strong, S. P., Koberle, R., and Bialek, W. (1997). Reproducibility and variability in neural spike trains. *Science* 275, 1805–1808.
68. Onken, A., Liu, J. K., Karunasekara, P. C. R., Delis, I., Gollisch, T., and Panzeri, S. (2016). Using matrix and tensor factorizations for the single-trial analysis of population spike trains. *PLoS computational biology* 12, e1005189.

69. McIntosh, L., Maheswaranathan, N., Nayebi, A., Ganguli, S., and Baccus, S. Deep learning models of the retinal response to natural scenes. In: *Advances in Neural Information Processing Systems (NeurIPS)* (2016):.
70. Zheng, Y., Jia, S., Yu, Z., Liu, J. K., and Huang, T. (2021). Unraveling neural coding of dynamic natural visual scenes via convolutional recurrent neural networks. *Patterns* 2, 100350.
71. Yamins, D. L., Hong, H., Cadieu, C. F., Solomon, E. A., Seibert, D., and DiCarlo, J. J. (2014). Performance-optimized hierarchical models predict neural responses in higher visual cortex. *Proceedings of the national academy of sciences* 111, 8619–8624.
72. Gerstner, W., and Kistler, W. M. Spiking neuron models: Single neurons, populations, plasticity. Cambridge university press (2002).
73. Vaswani, A., Shazeer, N., Parmar, N., Uszkoreit, J., Jones, L., Gomez, A. N., Kaiser, Ł., and Polosukhin, I. Attention is all you need. In: *Advances in neural information processing systems* vol. 30 (2017):.
74. Zhang, J., Dong, B., Zhang, H., Ding, J., Heide, F., Yin, B., and Yang, X. Spiking transformers for event-based single object tracking. In: *CVPR* (2022):( 8801–8810).
75. Masland, R. H. (2004). Neuronal cell types. *Current Biology* 14, R497–R500.
76. Klindt, D., Ecker, A. S., Euler, T., and Bethge, M. Neural system identification for large populations separating “what” and “where”. In: *Advances in Neural Information Processing Systems* vol. 30 (2017):.
77. Zhuang, C., Yan, S., Nayebi, A., Schrimpf, M., Frank, M. C., DiCarlo, J. J., and Yamins, D. L. (2021). Unsupervised neural network models of the ventral visual stream. *Proceedings of the National Academy of Sciences* 118, e2014196118.
78. Cadena, S. A., Denfield, G. H., Walker, E. Y., Gatys, L. A., Tolia, A. S., Bethge, M., and Ecker, A. S. (2019). Deep convolutional models improve predictions of macaque v1 responses to natural images. *PLoS computational biology* 15, e1006897.
79. Ratan Murty, N. A., Bashivan, P., Abate, A., DiCarlo, J. J., and Kanwisher, N. (2021). Computational models of category-selective brain regions enable high-throughput tests of selectivity. *Nature communications* 12, 5540.
80. Tal, D., and Schwartz, E. L. (1997). Computing with the leaky integrate-and-fire neuron: logarithmic computation and multiplication. *Neural computation* 9, 305–318.
81. Brunel, N., and Van Rossum, M. C. (2007). Lapicque’s 1907 paper: from frogs to integrate-and-fire. *Biological cybernetics* 97, 337–339.
82. Xiao, M., Meng, Q., Zhang, Z., He, D., and Lin, Z. Online training through time for spiking neural networks. In: *Advances in Neural Information Processing Systems (NeurIPS)* (2022):.
83. Van Kampen, N. G. Stochastic processes in physics and chemistry vol. 1. Elsevier (1992).
84. Kloeden, P. E., and Platen, E. Stochastic differential equations. In: *Numerical solution of stochastic differential equations* ( 103–160). Springer (1992):( 103–160).
85. Barndorff-Nielsen, O. E., and Shephard, N. (2001). Non-gaussian ornstein–uhlenbeck-based models and some of their uses in financial economics. *Journal of the Royal Statistical Society: Series B (Statistical Methodology)* 63, 167–241.

86. Patel, A., and Kosko, B. (2008). Stochastic resonance in continuous and spiking neuron models with levy noise. *IEEE Transactions on Neural Networks* 19, 1993–2008.
87. Plesser, H. E., and Gerstner, W. (2000). Escape rate models for noisy integrate-and-free neurons. *Neurocomputing* 32, 219–224.
88. Jolivet, R., Rauch, A., Lüscher, H.-R., and Gerstner, W. (2006). Predicting spike timing of neocortical pyramidal neurons by simple threshold models. *Journal of computational neuroscience* 21, 35–49.
89. Burt Jr, J. M., and Garman, M. B. (1971). Conditional monte carlo: A simulation technique for stochastic network analysis. *Management Science* 18, 207–217.
90. Titsias, M. K., Lázaro-Gredilla, M. et al. Local expectation gradients for black box variational inference. In: *Advances in Neural Information Processing Systems (NeurIPS)* (2015):.
91. Tokui, S., and Sato, I. Evaluating the variance of likelihood-ratio gradient estimators. In: *International Conference on Machine Learning*. PMLR (2017):( 3414–3423).
92. Fiete, I. R., and Seung, H. S. (2006). Gradient learning in spiking neural networks by dynamic perturbation of conductances. *Physical Review Letters* 97, 048104.
93. Shekhovtsov, A., Yanush, V., and Flach, B. Path sample-analytic gradient estimators for stochastic binary networks. In: *Advances in Neural Information Processing Systems (NeurIPS)* (2020):.
94. Shrestha, S. B., and Orchard, G. Slayer: Spike layer error reassignment in time. In: *Advances in Neural Information Processing Systems (NeurIPS)* vol. 31 (2018):.
95. Mao, X. Stochastic differential equations and applications. Elsevier (2007).
96. Cubuk, E. D., Zoph, B., Mane, D., Vasudevan, V., and Le, Q. V. Autoaugment: Learning augmentation policies from data. In: *CVPR* (2018):.
97. Samadzadeh, A., Far, F. S. T., Javadi, A., Nickabadi, A., and Chehreghani, M. H. (2020). Convolutional spiking neural networks for spatio-temporal feature extraction. *arXiv*.
98. Kingma, D. P., and Ba, J. (2014). Adam: A method for stochastic optimization. *arXiv*.
99. Loshchilov, I., and Hutter, F. (2016). Sgdr: Stochastic gradient descent with warm restarts. *arXiv*.
100. Zheng, H., Wu, Y., Deng, L., Hu, Y., and Li, G. Going deeper with directly-trained larger spiking neural networks. In: *Proceedings of the AAAI conference on artificial intelligence* vol. 35 (2021):( 11062–11070).
101. Fang, W., Yu, Z., Chen, Y., Huang, T., Masquelier, T., and Tian, Y. Deep Residual Learning in Spiking Neural Networks. In: *Advances in Neural Information Processing Systems (NeurIPS)* (2021):.
102. Lezcano-Casado, M. Trivializations for gradient-based optimization on manifolds. In: *Advances in Neural Information Processing Systems (NeurIPS)* (2019):( 9154–9164).
103. Goodfellow, I. J., Shlens, J., and Szegedy, C. Explaining and harnessing adversarial examples. In: *International Conference on Learning Representations* (2015):.



104. Fano, U. (1947). Ionization yield of radiations. ii. the fluctuations of the number of ions. *Physical Review* 72, 26.
105. Park, I. M., Seth, S., Paiva, A. R., Li, L., and Principe, J. C. (2013). Kernel methods on spike train space for neuroscience: a tutorial. *IEEE Signal Processing Magazine* 30, 149–160.
106. Arribas, D., Zhao, Y., and Park, I. M. Rescuing neural spike train models from bad mle. In: *Advances in Neural Information Processing Systems (NeurIPS)* vol. 33 (2020):( 2293–2303).
107. Zenke, F., and Ganguli, S. (2018). Superspike: Supervised learning in multilayer spiking neural networks. *Neural computation* 30, 1514–1541.